

Review

Influence of Energetic Particles and Electron Injection on Minority Carrier Transport Properties in Gallium Oxide

Sushrut Modak ¹, Arie Ruzin ², Alfons Schulte ^{1,3} and Leonid Chernyak ^{1,*}¹ Physics Department, University of Central Florida, Orlando, FL 32816, USA² School of Electrical Engineering, Tel Aviv University, Tel Aviv 69978, Israel³ College of Optics and Photonics, University of Central Florida, Orlando, FL 32816, USA

* Correspondence: leonid.chernyak@ucf.edu

Abstract: The influence of various energetic particles and electron injection on the transport of minority carriers and non-equilibrium carrier recombination in Ga₂O₃ is summarized in this review. In Ga₂O₃ semiconductors, if robust p-type material and bipolar structures become available, the diffusion lengths of minority carriers will be of critical significance. The diffusion length of minority carriers dictates the functionality of electronic devices such as diodes, transistors, and detectors. One of the problems in ultrawide-bandgap materials technology is the short carrier diffusion length caused by the scattering on extended defects. Electron injection in n- and p-type gallium oxide results in a significant increase in the diffusion length, even after its deterioration, due to exposure to alpha and proton irradiation. Furthermore, post electron injection, the diffusion length of an irradiated material exceeds that of Ga₂O₃ prior to irradiation and injection. The root cause of the electron injection-induced effect is attributed to the increase in the minority carrier lifetime in the material due to the trapping of non-equilibrium electrons on native point defects. It is therefore concluded that electron injection is capable of “healing” the adverse impact of radiation in Ga₂O₃ and can be used for the control of minority carrier transport and, therefore, device performance.

Keywords: gallium oxide; transport properties; minority carriers



Citation: Modak, S.; Ruzin, A.; Schulte, A.; Chernyak, L. Influence of Energetic Particles and Electron Injection on Minority Carrier Transport Properties in Gallium Oxide. *Condens. Matter* **2024**, *9*, 2. <https://doi.org/10.3390/condmat9010002>

Academic Editor: Amador Pérez Tomás

Received: 11 October 2023

Revised: 15 November 2023

Accepted: 2 January 2024

Published: 6 January 2024



Copyright: © 2024 by the authors. Licensee MDPI, Basel, Switzerland. This article is an open access article distributed under the terms and conditions of the Creative Commons Attribution (CC BY) license (<https://creativecommons.org/licenses/by/4.0/>).

1. Introduction

Semiconductors with a wide bandgap (WBG), among which gallium nitride and zinc oxide are notable examples, are of significant relevance for high-temperature electronics and for solar-blind ultraviolet radiation detection in the cosmos [1–3]. Novel gallium oxide semiconductors, with a direct forbidden gap of 4.7–4.9 eV (an ultrawide bandgap), are promising for applications in harsh environments in terms of their superior stability over their GaN and ZnO counterparts; this is due to their following unique combinations of physical properties [1,4–9]:

1. The above-mentioned ultrawide bandgap, which makes gallium oxide ideal for high-temperature and high-power applications;
2. Chemical stability: Ga₂O₃ is highly resistant to chemical corrosion, including exposure to acids, bases, and other corrosive chemicals;
3. Radiation hardness: Ga₂O₃ is resistant to radiation damage, making it suitable for use in space and other high-radiation environments;
4. Mechanical strength: Ga₂O₃ is a hard and durable material, making it suitable for use in demanding applications.

In addition to the above properties, Ga₂O₃ is also a relatively abundant and low-cost material, making it a promising candidate for commercialization.

P-type doping in gallium oxide has been a long-standing challenge due to its inherent self-compensation mechanism, which tends to neutralize any introduced acceptor impurities [7,9–12]. This self-compensation arises from the formation of compensating defects,

such as oxygen vacancies, which act as donors and counteract the p-type behavior. As a result, achieving stable and controllable p-type doping in Ga₂O₃ has been difficult, limiting its potential application in various electronic and optoelectronic devices.

Additionally, it has been revealed that the holes in β-Ga₂O₃ possess a high effective mass, as well as a low dispersion and high density of states. These factors dictate the creation of self-trapped holes [13–17], thus hindering p-type conductivity. Contrasting these claims, Ref. [10] reported the feasibility of defect engineering in grown β-gallium oxide facilitating hole conductivity at elevated temperatures, i.e., controlling the growth conditions can influence the formation and distribution of the defects in Ga₂O₃. By tailoring the defect structure, it became possible to reduce the self-compensation effect and to promote p-type conductivity.

The findings in Ref. [10] are in agreement with the results presented in Ref. [12], showing that the self-trapping nature of holes vanishes above 90–120 K. Accounting for the high interest in robust p-type doping in gallium oxide, it is expected that gallium oxide-based bipolar devices will soon become a reality.

Exploring acceptor dopants with relatively low ionization energies and higher solubility offers an alternative solution towards the performance of potentially effective p-type doping in Ga₂O₃. Very recently, Ref. [11] reported that gallium oxide doped with Zn exhibited room-temperature p-type conductivity.

While the above-referenced approaches have shown promise, achieving reliable and controllable p-type doping in Ga₂O₃ remains an ongoing research challenge. Overcoming this hurdle could open up new opportunities for Ga₂O₃-based devices, such as p–n junctions, bipolar transistors, and optoelectronic devices.

In Ga₂O₃ semiconductors, if bipolar structures become available, the diffusion length of minority carriers will be of critical significance. The diffusion length dictates the functionality of such electronic devices as diodes, transistors, and detectors [18]. One of the problems in wide-bandgap materials (e.g., gallium nitride and zinc oxide) technology is the short minority carrier diffusion length, which is caused by the scattering on extended defects [19,20]. At the same time, low-energy electron injection into p-type GaN and ZnO, using either an electron beam of a scanning electron microscope (SEM), the forward bias of Schottky barriers, or p–n junctions, leads to a drastic elongation of the minority electron diffusion length in these materials [19,21–24]. Similar effects were reported in n-type Ga₂O₃, using an SEM electron beam or solid-state electron injection (see below and Refs. [25,26]), and also in highly resistive p-type material [27]. An increase in the minority carrier diffusion length translated into changes in the luminescent characteristics of GaN, ZnO, and Ga₂O₃ [26,28–30], and into an experimentally demonstrated superior photovoltaic detector performance in the case of GaN and ZnO [18,24,31,32]; very recently, this was also demonstrated in the case of Ga₂O₃-based heterostructures.

It has also been discovered that, on the one hand, the irradiation of Si-doped β-Ga₂O₃ by 1.5 MeV electrons, 18 MeV α-particles, or 10 MeV protons leads to the deterioration of the minority carrier diffusion length and the minority carrier lifetime [25,33–35]. On the other hand, a low-energy SEM beam injection into an irradiated Ga₂O₃ Schottky barrier recovers/enhances minority carrier transport, as is expressed in the consequent long-lasting increase in the diffusion length [25–27,35]. It should be stressed that the diffusion length of irradiated gallium oxide samples after electron injection surpasses that prior to irradiation and injection. It is, therefore, possible to use an SEM beam (or forward bias) charge injection to improve a material's fundamental properties and, prospectively, the performance of devices made from that material, which are dependent on minority carrier transport and affected by radiation.

The main aim of this review article is to summarize the authors' previous results related to non-equilibrium minority carrier recombination (lifetime) and transport properties (diffusion length) in n-type and highly resistive π (p-type) β-gallium oxide epitaxial layers. These layers were grown either on Sn-doped Ga₂O₃ (n-type) or c-oriented sapphire substrates (π) and were subjected to various radiation types (energetic electrons;

gamma-, alpha-, and proton-irradiation); this led to the deterioration of minority carrier transport, and, separately, to low-energy electron beam exposure using a scanning electron microscope (SEM), as explained above. The latter exposure, in contrast to the irradiation of energetic particles, resulted in an enhancement of the minority carrier transport and lifetime, and to the recovery of adverse radiation impact. The enhancement of minority carrier transport using charge injection is a novel niche in wide and ultrawide-bandgap semiconductors, and the present review summarizes the current state of the art in the field.

The minority carrier lifetime and diffusion length characteristics summarized in this review are the two main parameters that represent carrier transport properties. They were independently measured using two different techniques in situ in SEM, namely electron-beam-induced current (EBIC) and time-resolved cathodoluminescence (TRCL). Additionally, new results presenting the impact of solid-state injection on the spectral photoresponse of NiO/Ga₂O₃ p–n heterojunctions are reported. The latter results serve as a proof of concept for the application of charge (either electron or hole) injection effects in optoelectronic devices, such as photodetectors, for controlling their photoresponse (collection efficiency) and mitigating radiation-induced defects.

The structure of this review is as follows:

1. The methodology employed for the diffusion length measurements taken in situ using the scanning electron microscope will be explained for the example of highly resistive p-Ga₂O₃;
2. The methodology employed for the electron beam probing of optical properties will be outlined, using the results for n-type Ga₂O₃ as an example;
3. The impact of various radiation types on minority carrier transport and optical properties will be reviewed;
4. The influence of SEM electron injection on minority carrier diffusion in Ga₂O₃ before and after exposure to radiation will be discussed;
5. The root cause for the phenomenon of electron injection in gallium oxide and its impact on minority carrier transport will be explained;
6. The application of the charge injection effect to the enhancement of the photoresponse in gallium oxide-based heterostructures will be considered as an example;
7. The main conclusions will be summarized.

2. Methodology

2.1. Electron-Beam-Induced Current Measurements of Minority Carrier Diffusion Length

EBIC is a powerful technique for imaging and characterizing semiconductor devices and materials. It offers high spatial resolution, quantitative analysis, and versatility. It is also non-destructive. However, it is also a relatively expensive and complex technique. Another potential disadvantage is related to its limited depth of penetration into the material under test. This penetration depth or electron range in the material depends on the mechanical density and SEM accelerating voltage [36].

The diffusion length of minority carriers was measured using the electron-beam-induced current (EBIC) technique on a scanning electron microscope (SEM). The diffusion length was relevant for electrons or holes depending on the electrical conductivity type. The measurements were carried out on Schottky contacts at a room-temperature (RT) range of -130 °C using a temperature-controlled stage installed in the SEM vacuum chamber. The electron beam accelerating voltage varied between 10 and 30 kV. The EBIC line scans were recorded on a planar structure, as shown in Figure 1. The signal was amplified using a Stanford Research Systems SR 570 low-noise current amplifier and digitized with a Keithley 2000 multimeter, which was controlled using homemade software.

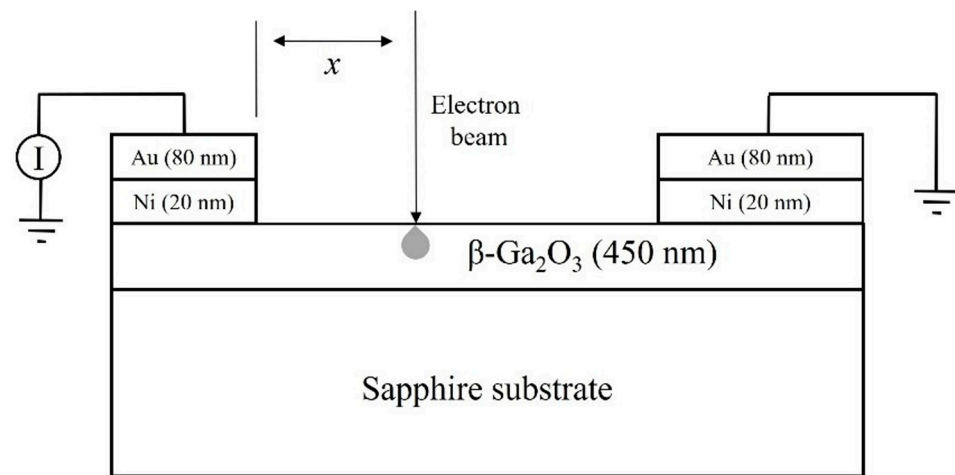


Figure 1. Schematics for EBIC measurements. Reprinted with permission from the AIP. After Ref. [36].

The diffusion length, L , was extracted from the EBIC line scans using the following equation [37–39]:

$$C(x) = C_0 x^\alpha \exp\left(-\frac{x}{L}\right) \tag{1}$$

Here, $C(x)$ is the electron-beam-induced current signal as a function of the coordinate; C_0 is a scaling factor; x is the coordinate counted from the edge of the contact stack; and α is a recombination coefficient (set at -0.5).

Figure 2 illustrates the methodology employed for the extraction of the minority carrier diffusion length using the example of two highly resistive p-type samples. Because of the low carrier concentration in the structures under test, the metal/semiconductor space-charge region (cf. Figure 1) was comparable or wider than the diffusion length. Hence, the methodology explained in Ref. [37] has been employed. Figure 2a,b show the raw data and their fit using Equation (1), which was employed for the extraction of L for two samples under test (samples A and B; A: $p = 5.6 \times 10^{14} \text{ cm}^{-3}$; $\mu = 8.0 \text{ cm}^2 \text{ V}^{-1} \text{ s}^{-1}$; B: $p = 2.7 \times 10^{13} \text{ cm}^{-3}$ and $\mu = 16 \text{ cm}^2 \text{ V}^{-1} \text{ s}^{-1}$). Meanwhile, the majority hole concentration and mobility for the above-referenced samples were measured at 850 K using the Hall effect setup; the EBIC testing was performed at 300–400 K.

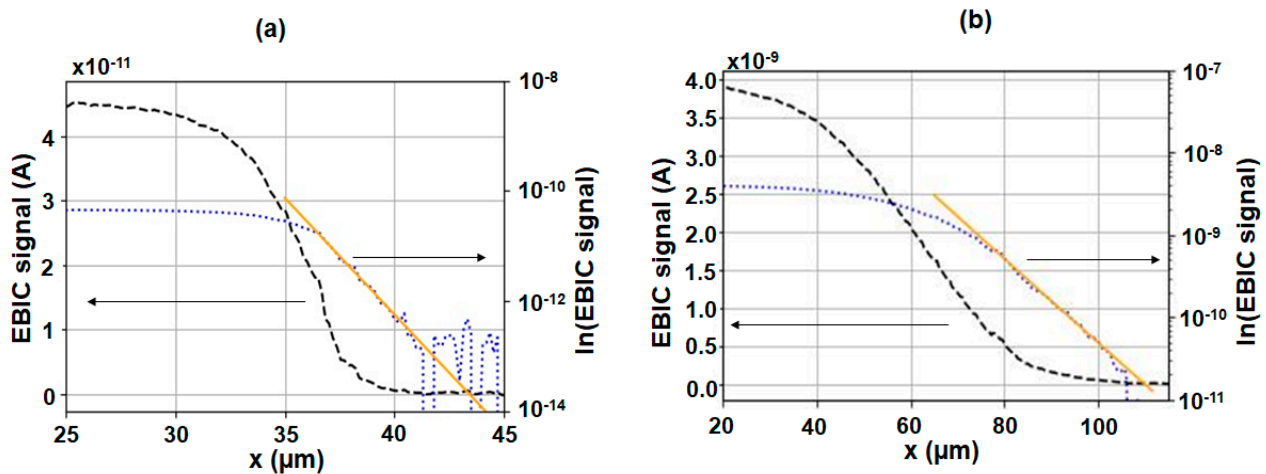


Figure 2. Raw data for the structure A (a) and the structure B (b) at RT, and the fit for the extraction of the diffusion length. Reprinted with permission from the AIP. After Ref. [36].

The dependence of the minority carrier diffusion length on temperature, T , for a highly resistive p-type material is demonstrated in Figure 3. The decrease in L with the rise in T is a typical trend observed in gallium oxide. The large values of L in Figure 3 are additional

indirect proof that the samples are p-type, as the minority carriers in this case are electrons, which possess much higher levels of mobility compared to holes. The latter have a large effective mass of $18.8 m_0$ [40]. L for minority carriers in n-gallium oxide is in the range of 50–600 nm [25,26,33,41,42], which is much lower than that reported in Ref. [36] for minority carrier electrons. Another reason for the large diffusion length values reported in Figure 3 is related to the low majority carrier concentrations in samples A and B and, therefore, the low scattering on electrically active impurities. Phonon scattering [40,43] may also play a role. It should be noted that a dependence similar to that of L on temperature in Figure 3 was found for n-type $\beta\text{-Ga}_2\text{O}_3$; this was ascribed to ionized impurity scattering due to heavy Si doping [33].

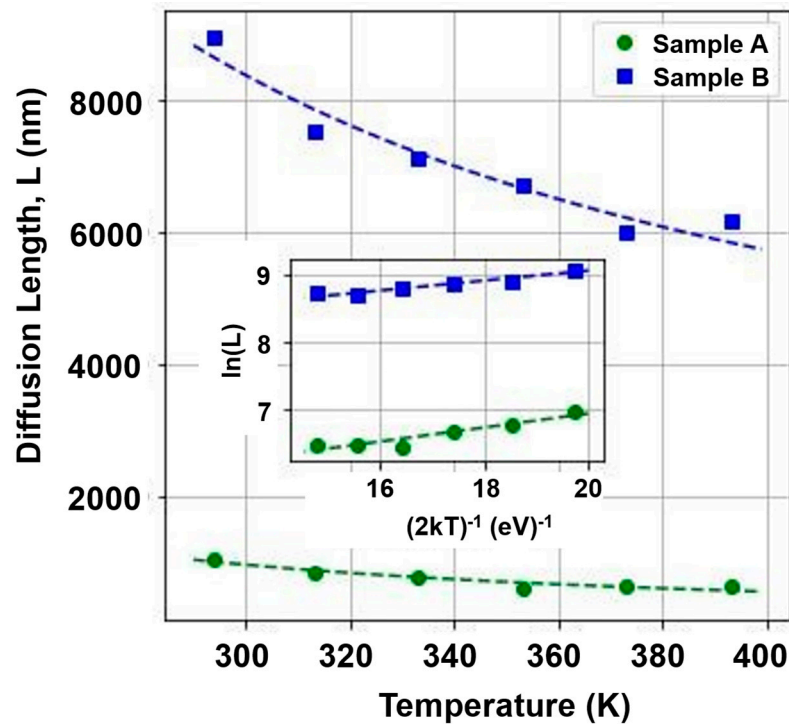


Figure 3. Dependence of the diffusion length on temperature for highly resistive p-type samples. Inset: Arrhenius plot and the fit for $\Delta E_{L,T}$. Reprinted with permission from the AIP. After Ref. [36].

The activation energy for the temperature dependence of L is given by the following [38]:

$$L(T) = L_0 \exp\left(\frac{\Delta E_{L,T}}{2kT}\right) \quad (2)$$

Here, L_0 is a scaling constant; $\Delta E_{L,T}$ is the thermal activation energy; k is the Boltzmann constant; and T is the temperature. The activation energies related to the decrease in L with temperature were found to be 67 meV (sample A) and 113 meV (samples B), respectively. The difference in the activation energies for samples A and B is mainly a result of the difference in their majority carrier concentrations; these were determined, in turn, by the partial pressure of oxygen, which was set during the epitaxial growth.

2.2. Continuous and Time-Resolved Cathodoluminescence

Cathodoluminescence (CL) is a versatile technique for measuring the emission of light from the material. It offers a greater spatial resolution in comparison to photoluminescence (PL). The electron beam energy is a parameter that can be tuned to change the probing depth (the range of electrons) in the material [44–46]. Like the EBIC technique (see above), CL is also non-destructive and can provide insight into the radiative recombination of non-equilibrium charge carriers. At the same time, CL is a relatively expensive technique that requires an SEM for electron beam excitation. Additionally, one of the limitations of

CL that researchers should be aware of is related to a possible change in the intensity of the emitted light due to the elongation of the non-equilibrium carrier lifetime; this is caused by continuous electron beam excitation (cf. Section 3.5 below).

Generally, luminescence quenches as the temperature increases and offers insight into the trap-levels that participate in the radiative recombination of the charge carriers. The CL vs. T relationship is as follows:

$$I(T) = I_0 / \left(1 + \sum_{i=0}^n A_i e^{-\Delta E_{Ai}/kT} \right) \quad (3)$$

Here, I_0 is 0 K intensity and is a fitting parameter; A_i is the scaling constant for the process described by the energy of activation ΔE_{Ai} ; k is the Boltzmann constant; and T is the temperature in Kelvin.

The time dependence of the luminescence can be studied in continuous mode with an uninterrupted electron/photon beam (continuous wave, CW, luminescence), or via excitation with very short (ps-to-fs) pulses of photons/electrons and by observing the decay of the various spectral components in the luminescence spectrum. Both PL and time-resolved PL (TRPL) require photons of energy that are greater than the bandgap to observe the near band edge (NBE) emission; otherwise, only a partial luminescence spectrum is observed. With CL and time-resolved CL (TRCL), the NBE emission can be seen even with very low beam energies. One limitation of CL and TRCL in particular is the upper limit on the maximum beam current. Depending on its absolute value, the saturation of the luminescence may not be seen.

The temporal nature of the luminescence decay can be represented in the spatial domain using a streak camera. The excitation source is synchronized with the streak camera and is able to count the number of photons emitted after a certain delay in the discrete intervals and represent them in the form of a streak image. Figure 4, left, shows an example of a streak image obtained for the Ga_2O_3 emission at around 380 nm. To extract the lifetime of the peak luminescent component, a narrow slice of the data in the region of interest is extracted and integrated along the y axis. The integrated decay plot around 380 nm is shown in Figure 4, right.

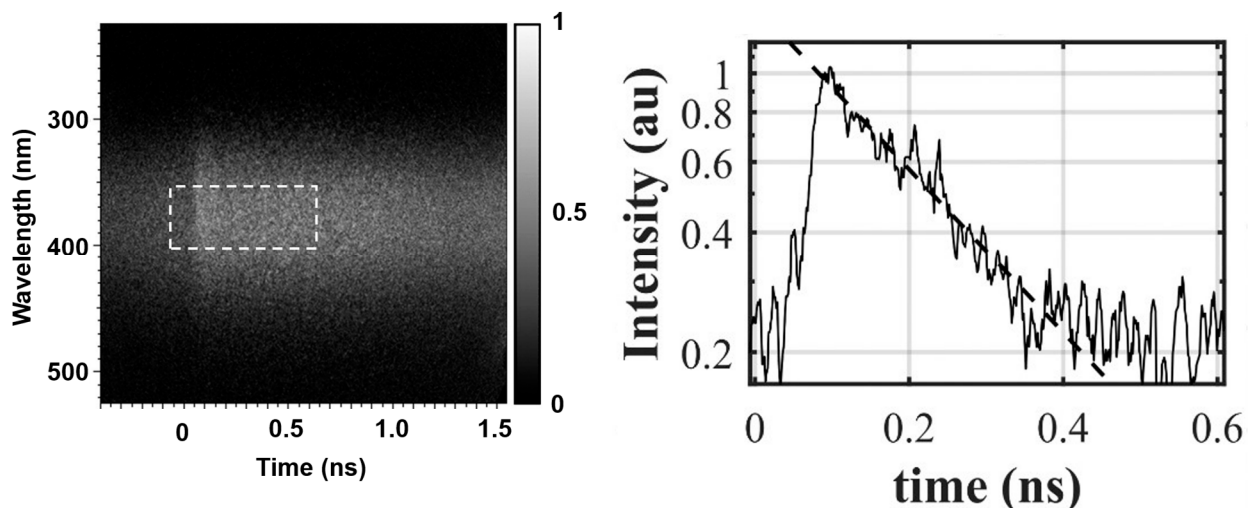


Figure 4. (Left): Time-resolved CL image from a streak camera with a center wavelength of 380 nm. The dashed rectangle shows the region for time decay determination. (Right): Normalized spectrum of CL decay at 380 nm with an exponential fit for n-type $\beta\text{-Ga}_2\text{O}_3$. The lifetime is obtained from the exponential fit inverse slope for the temporal CL decay. Reprinted with permission from the AIP. After Ref. [33].

The lifetime can be obtained from a fit to the equation:

$$A(t) = A_0 \exp(-t/\tau) + C \tag{4}$$

Here, A_0 is a constant related to the initial luminescence intensity; t is the time delay following excitation; τ is the lifetime; and C is the constant, which is associated with CL, persisting for longer than the excitation period.

Most of the continuous and time-resolved CL measurements summarized in this review, as well as some of the EBIC measurements, were carried out using the Attolight Allallin 4027 Chronos SEM-CL set up (cf. Figure 5). This system is equipped with a hybrid thermionic field emission electron gun with an accelerating energy of up to 10 keV. The CL signal, generated in response to the electron beam bombardment, is collected by a 360° parabolic mirror, which is placed near the pole piece of the electron beam column to maximize the collection efficiency. The mirror assembly is spatially coupled to a Horiba iHR 320 spectrometer, which is equipped with a 150 grooves/mm grating (blazed at 500 nm).

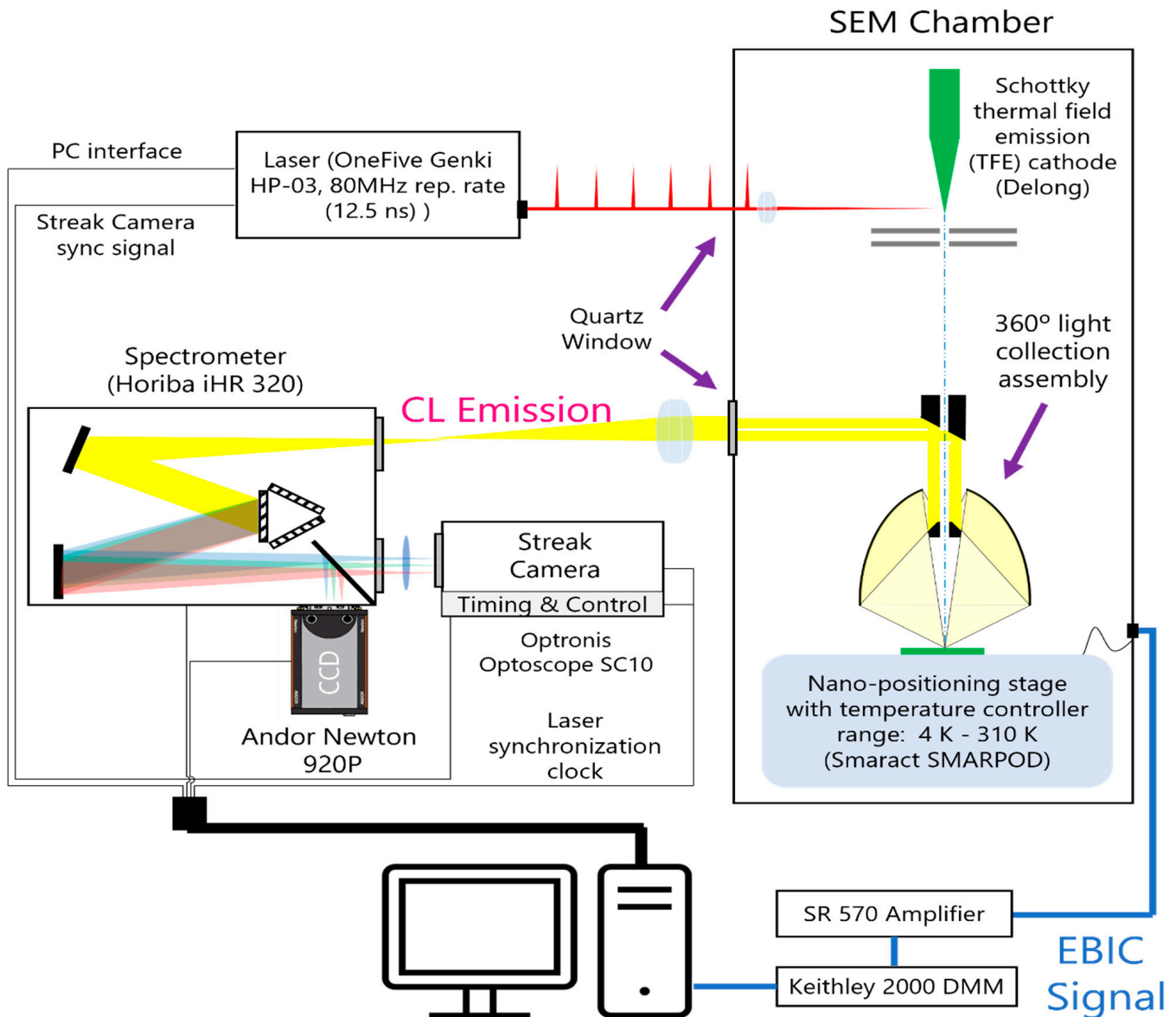


Figure 5. Experimental setup of the Attolight Allallin 4027 Chronos SEM-CL tool capable of sustaining temperatures from 4 K to 310 K.

Two separate imaging devices are attached to the exit of the spectrometer (they can be selected using a movable mirror): Andor Newton 920p CCD camera (180–1100 nm), with a resolution of 256×1024 pixels, and the Optronis Optoscope SC-10 streak camera, with a temporal resolution of 2 ps and an image resolution of 1200×1000 pixels. Under the continuous cathodoluminescence mode of operation, the sample is continuously bombarded with an electron beam, and the resulting cathodoluminescence signal, after being spectrally resolved by the spectrometer, is detected by the CCD camera. The integration time of the CCD can be varied from 10^{-4} s to 1 s, depending on the signal intensity and the noise level. The time-resolved mode is achieved by reducing the heating current of the tip of the electron gun filament just under the electron emission threshold. The remaining energy for the emission of the electrons is then supplied with the help of a femtosecond laser, which is focused on the electron gun tip. The femtosecond laser is operated in synchronization with the streak camera. Based on the photon energy threshold cutoff, streak images are obtained via integration over several dozens of electron beam excitation pulses. The maximum measurable duration of the signal that is recordable by the streak camera is 2 ns, and the excitation electron pulses are generated every 12.5 ns. It is, therefore, possible to extract the lifetime of various spectral components from the recorded streak image.

3. Impact of Radiation and Electron Injection on Minority Carrier Recombination

The below sections summarize the impacts of high-energy particles on minority carrier transport and the optical properties of Si-doped n-type β -Ga₂O₃. Additionally, minority carrier transport in undoped highly resistive p-Ga₂O₃ that was irradiated using protons with an energy sequence of 25–50–70 keV will be discussed. In the following sections, the effect of electron injection on the highly resistive p-Ga₂O₃ and the n-type gallium oxide will be considered, and the model will be presented. Finally, the application of the charge injection effect to bipolar NiO/Ga₂O₃ structures will be demonstrated.

3.1. Impact of Energetic Electron Bombardment on Minority Carrier Recombination

In Ref. [33], the EBIC, CWCL, and TRCL techniques were employed to investigate the effects of energetic electron irradiation on L and τ in n-type β -Ga₂O₃.

The samples under test were represented by epitaxial n-type β -Ga₂O₃ layers (Si-doped; electron concentration of $\sim 2 \times 10^{16}$ cm⁻³) that were grown via hydride vapor phase epitaxy (HVPE) on Sn-doped β -Ga₂O₃ substrates (electron concentration of $\sim 3.6 \times 10^{18}$ cm⁻³) [47]. The original epi-layer thickness of ~ 20 μ m was subsequently reduced via chemical mechanical polishing to a final thickness of 10 μ m.

Schottky diodes were fabricated using the e-beam evaporation of top rectifying and bottom Ohmic contacts, as shown in Figure 6. Current–voltage (I–V) measurements were carried out before and after irradiation with energetic electrons. Sample irradiation at 1.5 MeV (with fluences of 1.79×10^{15} and 1.43×10^{16} cm⁻² at a current of 1 mA) was performed at The Korea Atomic Energy Research Institute.

L was measured using EBIC in the planar configuration [20–22]. The EBIC line scan was recorded in situ over 10 s using a Philips XL-30 SEM at an accelerating voltage of 20 kV; this was as a function of the coordinate x , as depicted in Figure 6. Each single EBIC measurement was carried out on an unexposed region [20–22]. The EBIC was recorded for temperatures ranging from 295 to 395 K using a temperature-controlled stage.

L was extracted from Equation (1) by fitting the EBIC line scans [32,33]. The dependence of L vs. T is presented in Figure 7 for the irradiated and non-irradiated samples as a function of temperature, as described by Equation (2). The decrease in the diffusion length with temperature is ascribed to increased scattering or recombination due to traps. $\Delta E_{L,T}$, obtained from Equation (2), was approximately 40.9 meV for the non-irradiated sample, and much lower for the irradiated ones, showing activation energies of 18.1 and 13.6 meV; this is consistent with higher irradiation doses. Irradiation-induced traps likely reduce L due to increased recombination.

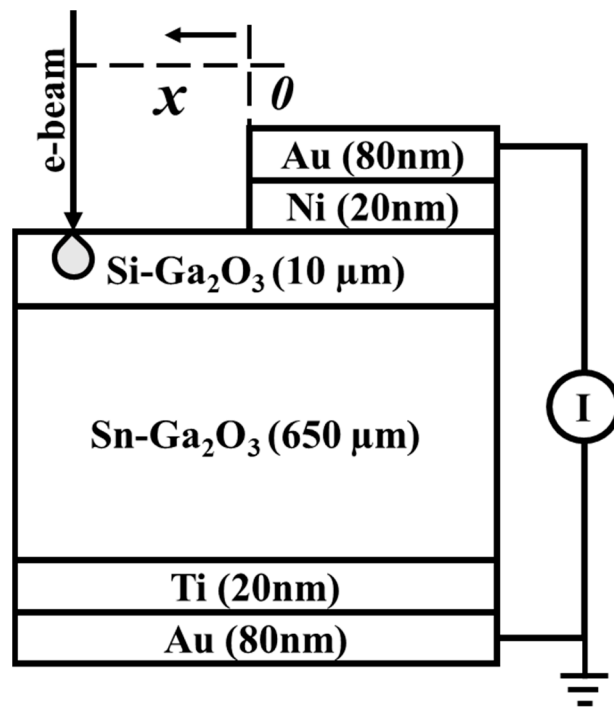


Figure 6. Vertical Schottky rectifiers used for EBIC measurements.

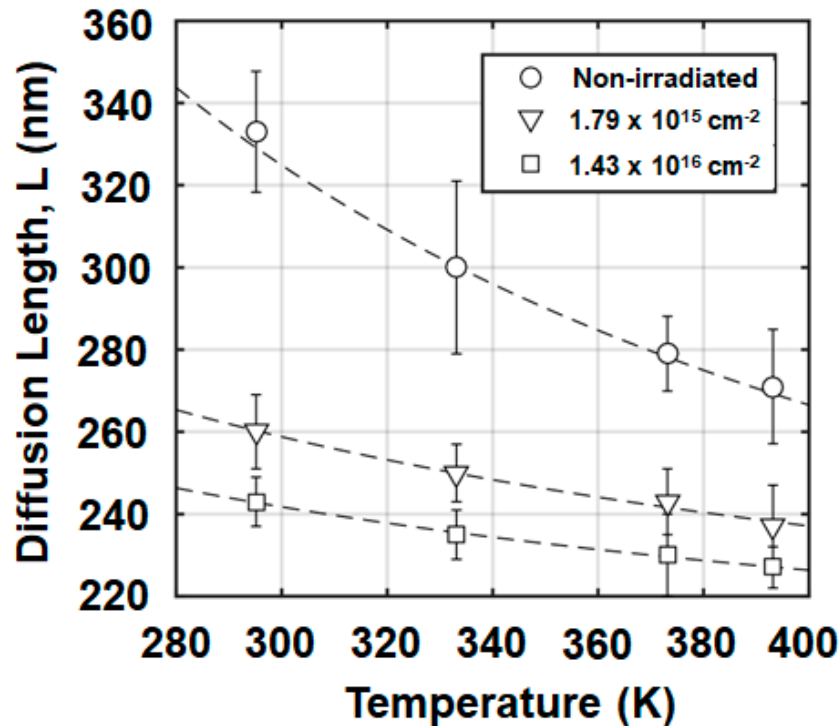


Figure 7. Dependence of L on T for irradiated and reference samples with fits, revealing the activation energy, $\Delta E_{L,T}$. Reprinted with permission from the AIP. After Refs. [32,33].

The continuous wave CL spectrum, which is presented in Figure 8, shows no band-edge emission at 255 nm (4.9 eV). It exhibits, instead, a wide spectrum with a peak of ~ 380 nm (~ 3.26 eV) and an 80 nm full-width at half-maximum (FWHM) bandwidth. According to the computational results of Ref. [12], the prevalence of self-trapped holes throughout $\beta\text{-Ga}_2\text{O}_3$ prevents band-edge recombination and p-type doping, and instead

the emission arises from the recombination caused by donor–acceptor pairs [12,13,43,48–54]. Neither high-resolution imaging in secondary electrons nor polychromatic cathodoluminescence revealed any surface changes, thus confirming the lack of modifications in the structure of β -Ga₂O₃ induced because of high-energy electron irradiation.

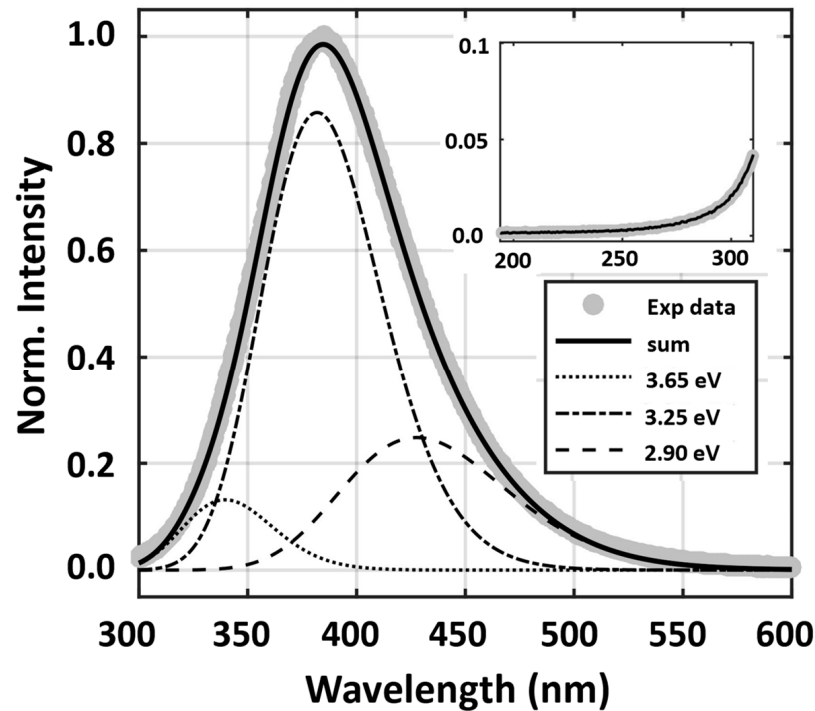


Figure 8. RT cathodoluminescence spectrum with a Gaussian decomposition, exhibiting bands at 3.65, 3.25, and 2.95 eV and no band-to-band emission (inset). Reprinted with permission from the AIP. After Refs. [32,33].

As shown in Figure 9, time-resolved CL measurements were performed within a 360–380 nm wavelength width. The TRCL signal is described by an exponential decay in agreement with Equation (4). The values of the lifetime reduced from 215 ps for the non-irradiated sample to 151 and 138 ps for the irradiated ones, thus confirming that the reaction to radiation results in an increase in the recombination rate. The lifetimes reported in Ref. [33] are much faster than those of ~30 ns found elsewhere using time-resolved photoluminescence (TRPL) [54,55]. In those studies, TRPL decay was observed to persist for a much longer time, with two distinct ranges for $\tau < 1 \mu\text{s}$ and $\tau > 1 \mu\text{s}$. The former range indicates that the short-lived ultrafast dynamics may differ from those found closer to equilibrium.

The minority carrier diffusion length is related to the lifetime and mobility of the non-equilibrium carriers via the Einstein relation:

$$L = \sqrt{D\tau} = \sqrt{\mu kT\tau/q} \quad (5)$$

Here, q is the electron charge. The carrier mobility, calculated at RT from Equation (5), decreased from 204 to 176 and ultimately to 166 $\text{cm}^2\text{V}^{-1}\text{s}^{-1}$ because of an increase in the dose for the 1.5 MeV electron bombardment. The mobility for holes reported in Ref. [33] is comparable to the electron mobility (153 $\text{cm}^2\text{V}^{-1}\text{s}^{-1}$), and is related to the short recombination lifetimes observed under fs-laser excitation in time-resolved CL experiments.

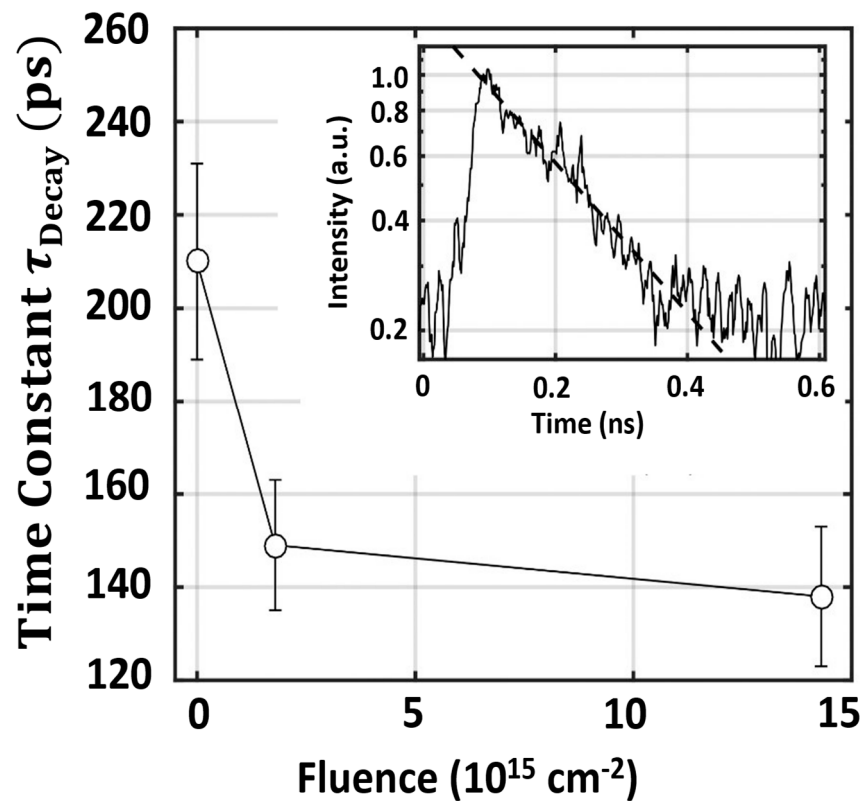


Figure 9. CL lifetime constant (open circles) for non-irradiated and irradiated samples. The inset shows a CL transient for a non-irradiated sample and an exponential fit (dotted line). Reprinted with permission from the AIP. After Refs. [32,33].

The pre-irradiation activation energy $\Delta E_{L,T}$ of 40.9 meV [33] is in good agreement with the donor ionization energy reported elsewhere [54,56–59], and is attributed to oxygen vacancies (V_{O}). Additionally, pairing is possible between the oxygen vacancies and nearby gallium vacancies that act as acceptors [44]. The reduction in the minority carrier diffusion length and $\Delta E_{L,T}$, which is induced by radiation, is ascribed to the creation of additional trap states between the conduction band and the shallow donor level, which act as an alternative recombination pathway; this is confirmed by the experimentally observed reduction in the lifetime. The possible radiation-induced traps are related to the displacement of oxygen atoms, which, in turn, results in V_{O} , pairs of V_{O} and V_{Ga} , or complexes of both.

To summarize this subsection, the irradiation of n-type gallium oxide with highly energetic electrons (1.5 MeV) led to a significant reduction in the minority carrier (holes) diffusion length and lifetime. This reduction was associated with the generation of defects that impacted the minority carrier transport. The lifetime for non-equilibrium carriers was measured using the time-resolved CL to study the impact of irradiation on the ultrafast recombination rate. While the pre-irradiation activation energy for L on T dependence was related to the shallow donor levels in the $\beta\text{-Ga}_2\text{O}_3$ samples, the samples subjected to radiation exhibited a reduction in their activation energy caused by additional radiation-induced trap states, as is also evidenced by the reduction in the lifetime.

3.2. Non-Equilibrium Carrier Recombination in Beta Gallium Oxide Irradiated with Alpha Particles and Protons

In Ref. [34], the non-equilibrium minority carrier dynamics were studied using EBIC and TRCL in Ga_2O_3 n-type samples subjected to alpha and proton irradiation. The structures, like those described in Section 3.1 and Figure 6, were used in the experiments. For the Schottky contacts under test, the calculated maximum electric field was 0.1 MV/cm at zero bias [60], and the barrier height was estimated at 1.08 V [61].

Several samples were selected for 10 MeV ($5 \times 10^{14} \text{ cm}^{-2}$ fluence; 330 μm range in the material) irradiation with protons and 18 MeV ($1 \times 10^{12} \text{ cm}^{-2}$ fluence; 80 μm range in the material) irradiation with alpha particles. The beam current of the cyclotron (Korean Institute of Radiological and Medical Science) was 100 nA in the case of both irradiation types. The removal rates for the carriers in the proton-irradiated and alpha-irradiated structures were around 240 cm^{-1} and 400 cm^{-1} , respectively. More details are outlined in Refs. [62,63].

The dependence of the minority carrier diffusion length on temperature for all the above-referenced samples (diodes) is shown in Figure 10. $\Delta E_{L,T}$ was extracted from Equation (2), with the values for the control, alpha-, and proton-irradiated diodes being 5.4, 4.1, and 3.7 meV, respectively, thus showing a modest dependence on temperature. In the previous investigations of GaN [22,23,38,45,64–67], Ga_2O_3 [25,26,35,68,69], and ZnO [19,24], larger $\Delta E_{L,T}$ values were ascribed to traps in the forbidden gap. The reduced (with increasing temperature) activation energy, as reported in Ref. [34] and shown in Figure 10, is likely related to a more pronounced carrier recombination. An additional factor that contributes to the low values of $\Delta E_{L,T}$ is attributed to the relatively small value of the minority carrier diffusion length in Ref. [34] in comparison to other reported values [33,39]. The above-referenced factors (as well as the relatively low electron beam current used in the experiments; see below) also represent the likely reasons for a small difference in the minority carrier diffusion length values obtained for the control, proton-, and alpha-irradiated samples in Figure 10. A lower electron beam current was used in Ref. [34] to minimize the impact of electron-injection-induced effects on the minority carrier diffusion length. These effects will be separately discussed in Sections 3.4 and 3.5 of this review.

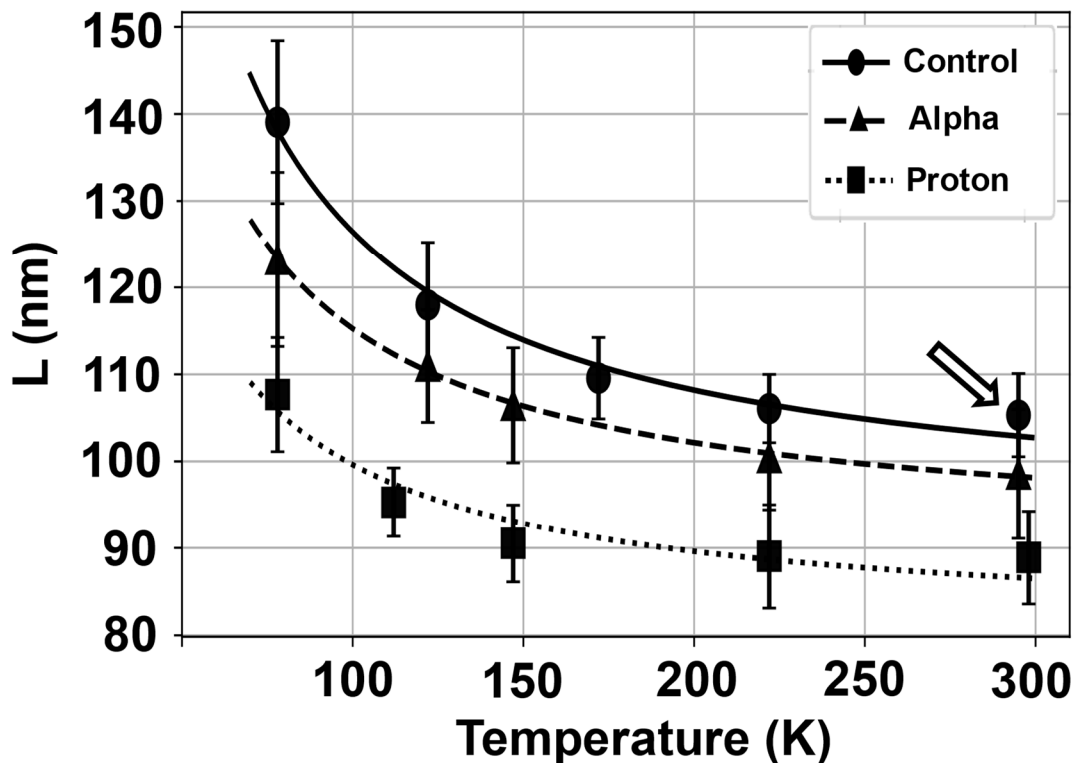


Figure 10. Temperature dependence of L for various radiation types. The arrow shows the RT values. Reprinted with permission from the AIP. After Ref. [34].

The time-resolved CL streak of the UV emission, which is centered around 380 nm in $\beta\text{-Ga}_2\text{O}_3$, is presented in Figure 11 (with continuous CL spectra reported in Ref. [33]); it is in agreement with a single exponential decay described by Equation (4).

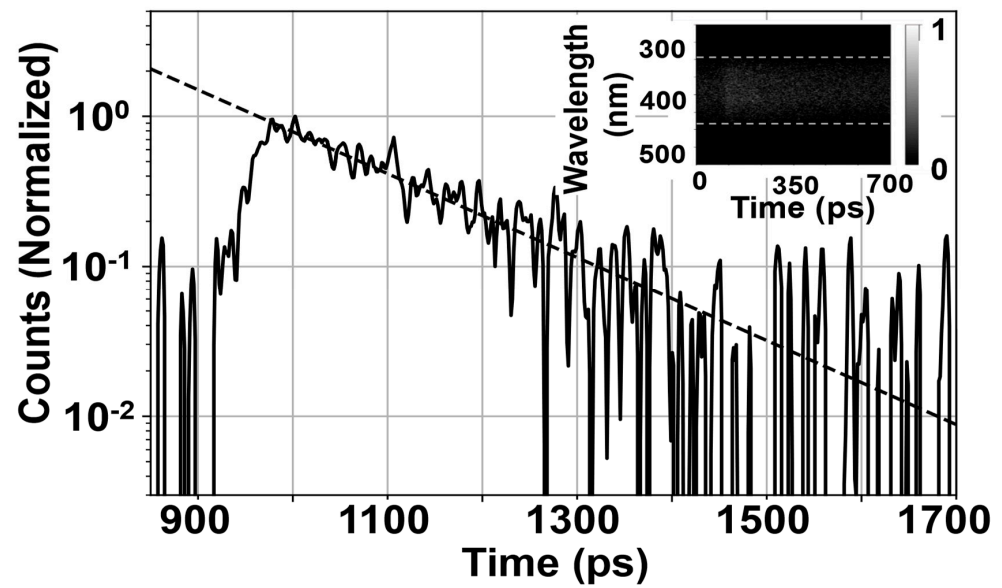


Figure 11. A streak of time-resolved CL, acquired at RT for the reference structure, and its raw image (inset). Reprinted with permission from the AIP. After Ref. [34].

The lifetime, τ , exhibits a decrease from 572 ps to 464 ps; this is via the intermediate value of 523 ps at 77 K for the control, α -, and proton-treated samples, respectively (Figure 12). The room temperature values are, correspondingly, 168 ps, 159 ps, and 154 ps. The measured room temperature value of the lifetime for the control sample is in agreement with that of 215 ps, as previously reported in Ref. [33]. The irradiated diodes experience the creation of additional point defects due to radiation damage and, therefore, demonstrate a decrease in the minority carrier diffusion length and lifetime [26,27,33,42,69–71]. L and τ were largest for the control diode, followed by the alpha- and proton-irradiated structures. This was explained by the fluence of protons being 500 times larger than the alpha irradiation.

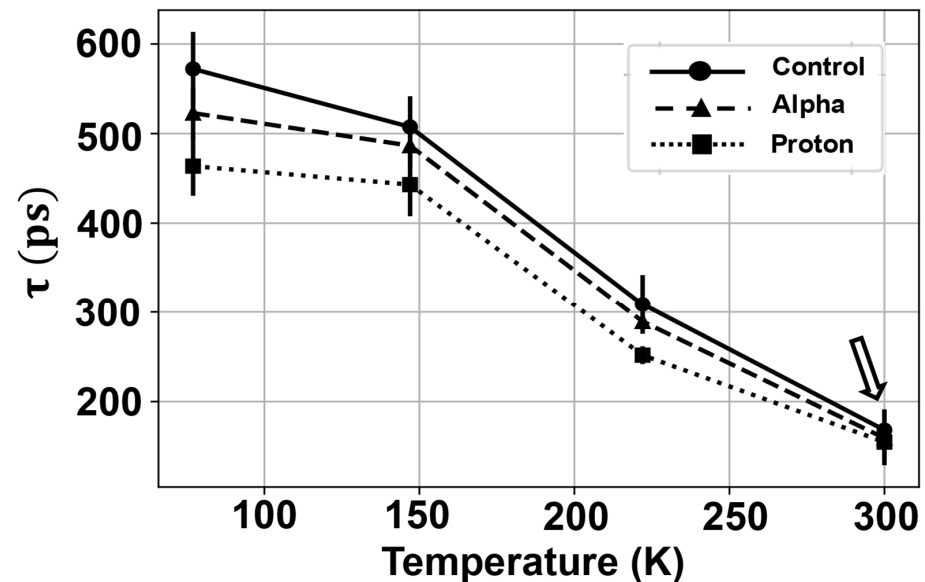


Figure 12. Lifetime vs. temperature dependence for structures irradiated by various particles. The arrow shows the RT value. Reprinted with permission from the AIP. After Ref. [34].

3.3. Minority Carrier Transport and Radiation Impact in Undoped Highly Resistive Ga_2O_3

Undoped and highly resistive 450 nm-thick β - Ga_2O_3 epitaxial layers were tested in Refs. [27,36] by using the EBIC technique. The epitaxial layers were grown using

metal–organic chemical vapor deposition, with further details regarding their growth and characterization outlined in Refs. [10,11].

The samples under test were denoted as **A** and **B** (cf. Section 2.1 for additional details). For these samples, the temperature dependence of L is shown in Figure 3. The minority carrier diffusion length decreased as T increased in these samples, with values for **A** and **B** of 1040 and 8506 nm at 304 K, respectively, and 640 and 6193 nm at 404 K, respectively. The fairly long minority carrier diffusion length in the above-referenced samples was partially ascribed to the low majority carrier concentrations (cf. Section 2.1 for values). The reduction in L with T was attributed to phonon scattering [40]. As has already been mentioned, the minority carrier (holes) diffusion length in n-type β -Ga₂O₃ is within the 50–600 nm range [25,26,33,39,41] and is lower than that for minority carrier electrons, as reported in Ref. [36]. One of the explanations for this experimental finding is related to a large (18.8 m_0) effective mass for holes [43]. A similar dependence of L on T is revealed in n-type β -gallium oxide, and it is linked to scattering on ionized Si impurities (due to heavy doping) [33].

$\Delta E_{L,T}$, extracted using Equation (2) and related to a decrease in L with T (cf. Figure 3), was found to be 67 meV (sample **A**) and 113 meV (sample **B**). This activation energy matches that of the thermal quenching of CL intensity (ΔE_{CL}): 67 and 88 meV for sample **A** ($\Delta E_{L,T}$ and ΔE_{CL} , respectively), and 113 and 101 meV for sample **B** ($\Delta E_{L,T}$ and ΔE_{CL} , respectively). The proximity of the values for $\Delta E_{L,T}$ and ΔE_{CL} is proof that the processes have the same origin; this is likely related to the thermal de-trapping of electrons from the $V_{Ga}-V_{O^{++}}$ complexes, thus creating acceptor levels in the Ga₂O₃ forbidden gap.

A series of separate EBIC measurements that showed comparable or higher (relative to the samples **A** and **B**) free hole concentrations was carried out on another Ga₂O₃ sample [27]. The sample was subjected to high-energy proton irradiation (cf. Figure 13 for doses and energies), with L measurements carried out prior to and following the exposure to the proton beam, as demonstrated in Figure 13. $\Delta E_{L,T}$ was found at 76 meV after irradiation (113 meV prior to irradiation). A discussion related to the decrease in the activation energy is outlined in Section 3.2.

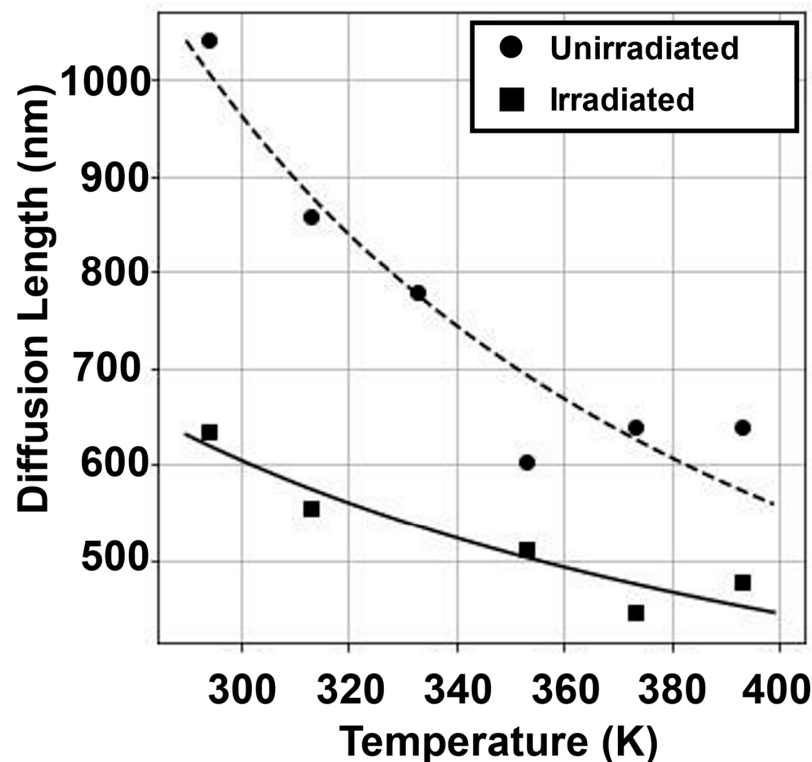


Figure 13. L vs. T dependence prior to and following bombardment with high-energy protons with the following energy/dose sequence: 25 keV, $1.6 \times 10^{14} \text{ cm}^{-2}$ + 50 keV, $1.7 \times 10^{14} \text{ cm}^{-2}$ + 70 keV, $3.6 \times 10^{14} \text{ cm}^{-2}$. Reprinted with permission from the AIP. After Refs. [27,36].

3.4. Electron Injection Impact of Minority Carrier Diffusion and Optical Properties on Ga₂O₃

A single EBIC line scan, needed for the extraction of L , lasts approximately 10–12 s. For electron injection in the region of diffusion length measurements, the motion of an electron beam is continuous for up to ~350 s (42.8 pC/μm³ injected charge density) [27], with the diffusion length being extracted intermittently. Note that the electrons of the SEM beam, which facilitate the generation of non-equilibrium electron–hole pairs in Ga₂O₃, are not accumulated in the sample due to the transition of excited electrons from the valence to the conduction band, as it is grounded. The electroneutrality is, therefore, preserved.

Ref. [72] reported that the radiation ionization energy needed for electron–hole pair creation is ~16 eV for β-Ga₂O₃. Considering that the density of the injected charge is ~43 pC/μm³ and that ~625 electron–hole pairs are generated in this volume (10,000 eV/16 eV), a ~10²³ cm⁻³ non-equilibrium density for the electron–hole pairs was obtained for the experimental regimes of the work outlined in Ref. [27]. Hence, the L values given in this sub-section are relevant to the non-equilibrium carriers that have concentrations significantly higher than those obtained from the Hall effect measurements. In the electron beam proximity (during the EBIC measurements), the number of non-equilibrium majority and minority carriers is equal (the concentration for both carriers significantly exceeds the equilibrium Hall majority carrier concentration at a given T), thus avoiding a high injection level regime [27].

Figure 14 shows L vs. the duration of electron injection dependence at variable temperatures for highly resistive p-Ga₂O₃. L increases linearly with the duration of electron injection before saturation (not shown in Figure 14). This linear increase in the minority carrier diffusion length with the injection duration was reported in Ref. [22] for p-GaN, in Ref. [19] for p-ZnO, in Ref. [45] for unintentionally doped GaN, and in Ref. [26] for n-Ga₂O₃.

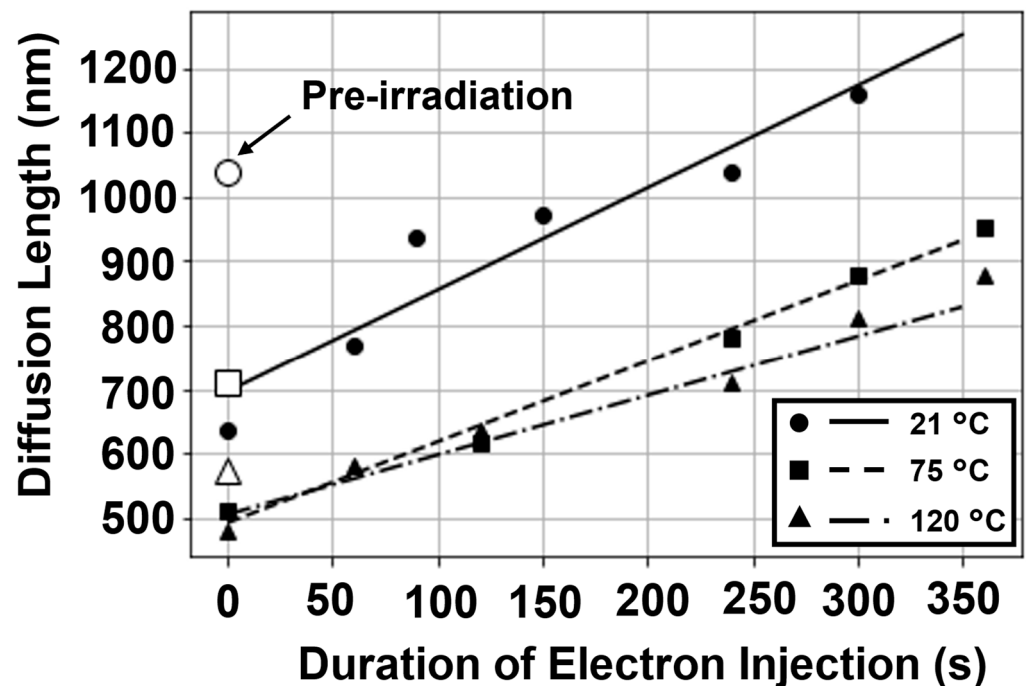


Figure 14. L vs. duration of electron injection dependence at variable temperatures for highly resistive p-Ga₂O₃. The L values for 0 injected charge are shown in an open circle (21 °C), square (75 °C), and triangle (120 °C). $\Delta E_{A,L}$, obtained from the dependence of L on the injection duration at varying T , is estimated at 91 meV using Equation (6). Reprinted with permission from the AIP. After Ref. [27].

The rate R (dL/dt , where t is the duration of electron injection) characterizes the increase in L in Figure 14. R decreases from 2 nm/s at room temperature to about 1 nm/s at 120 °C. The dependence of R on T is described by the following [19]:

$$R = R_0 \exp\left(\frac{\Delta E_{A,I}}{kT}\right) \exp\left(-\frac{\Delta E_{A,T}}{2kT}\right) \quad (6)$$

Here, R_0 is a scaling constant, and $\Delta E_{A,I}$ is the activation energy for the electron injection effect.

Equation (6) was employed in Ref. [27] to find the $\Delta E_{A,I}$ component for the increase in L using the Arrhenius plot in the inset of Figure 15, which shows a decrease in R as the temperature increases. The Arrhenius plot slope is defined as $\Delta E_{A,I} + 0.5 \Delta E_{A,T}$, from which an $\Delta E_{A,I}$ of ~91 meV was obtained. $\Delta E_{A,I}$ is related to the mechanism responsible for the elongation of the minority carrier diffusion length with injected charge. It was suggested that the observed effect is associated with the gallium vacancy (V_{Ga}), which is a dominant point defect in undoped Ga_2O_3 .

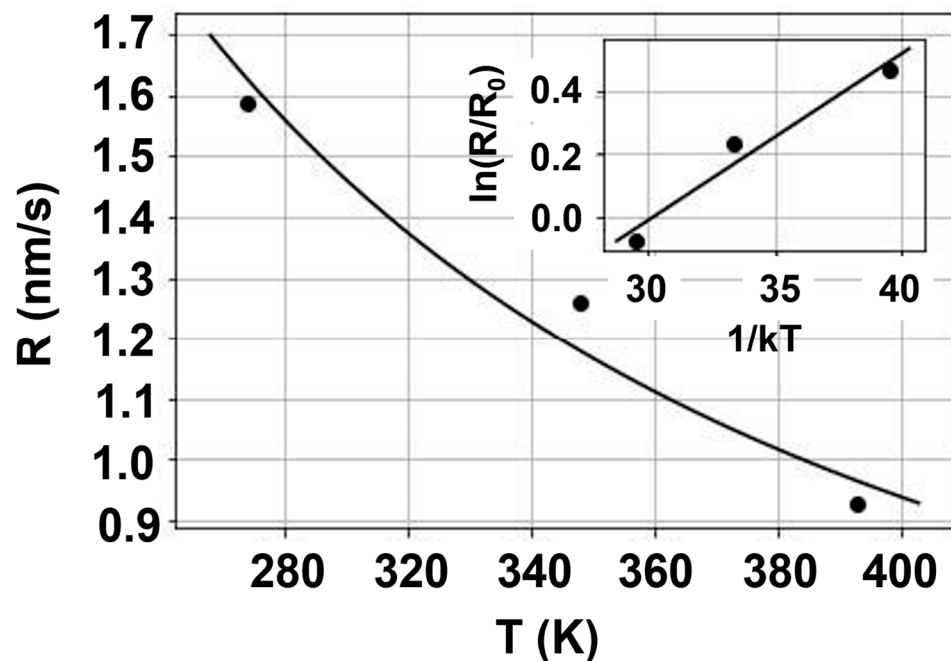


Figure 15. R vs. T dependence. Inset: Arrhenius plot of Equation (6) for the calculation of $\Delta E_{A,I}$. Reprinted with permission from the AIP. After Ref. [27].

Figure 14 proves that the negative influence of proton irradiation on L can be fully restored using electron injection. Furthermore, at respective temperatures, L in the irradiated material can increase above the pre-irradiation values.

The dynamics involved in the increase in L relaxation to the base level were investigated at RT after stopping the electron injection, which lasted up to about 350 s. L was found to stay unchanged for at least several days.

The RT CL spectra before and after proton bombardment are shown in Figure 16. A thorough investigation of the optical properties of highly resistive gallium oxide was recently published by the authors of this review in Ref. [36]. The narrower FWHM luminescence spectrum after proton bombardment, which is shown in Figure 16, was ascribed to the various complexes (point defects) that were created between V_{Ga} and hydrogen and incorporated during proton exposure. These point defects likely led to a reduction in the strain broadening of the observed luminescence [73] with no additional changes, both in terms of shape and intensity; this indicates that the injection-related increase in the lifetime for non-equilibrium carriers is mostly non-radiative.

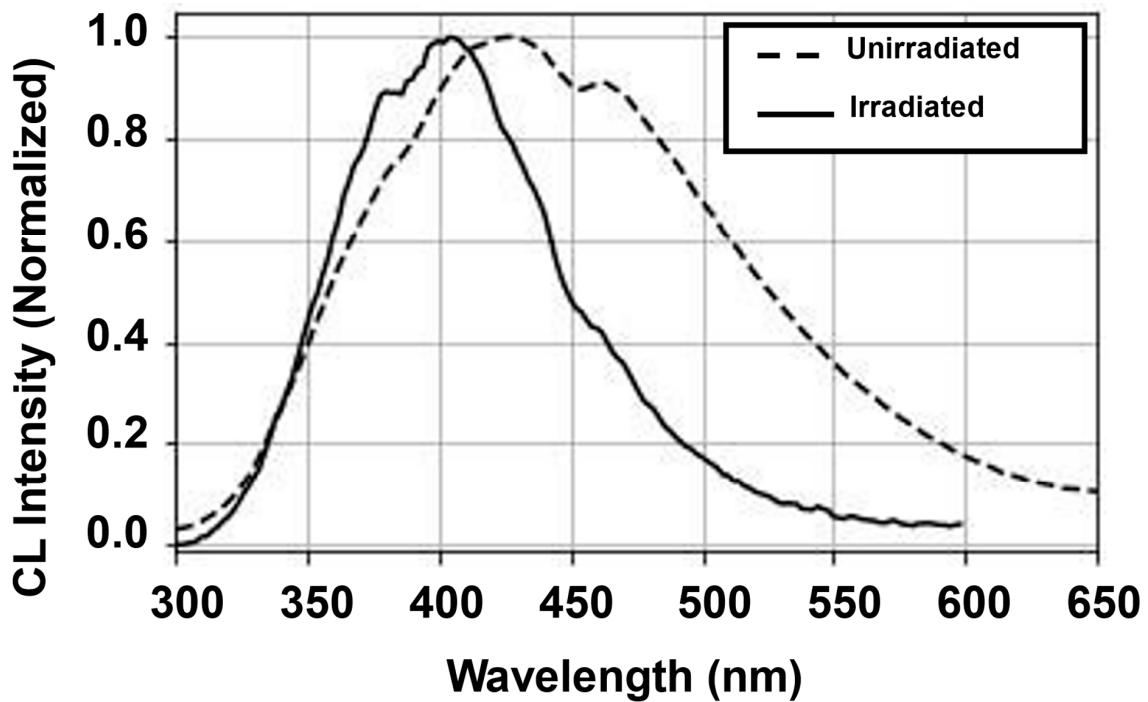


Figure 16. Normalized continuous RT CL spectrum before and after proton irradiation. A blue shift and smaller full-width at half-maximum (FWHM) were observed for the CL spectrum after irradiation. Reprinted with permission from the AIP. After Ref. [27].

Results similar to those in Figure 14 were obtained for the n-type Ga₂O₃ (under similar electron beam excitation conditions) and are presented in Figure 17 [26].

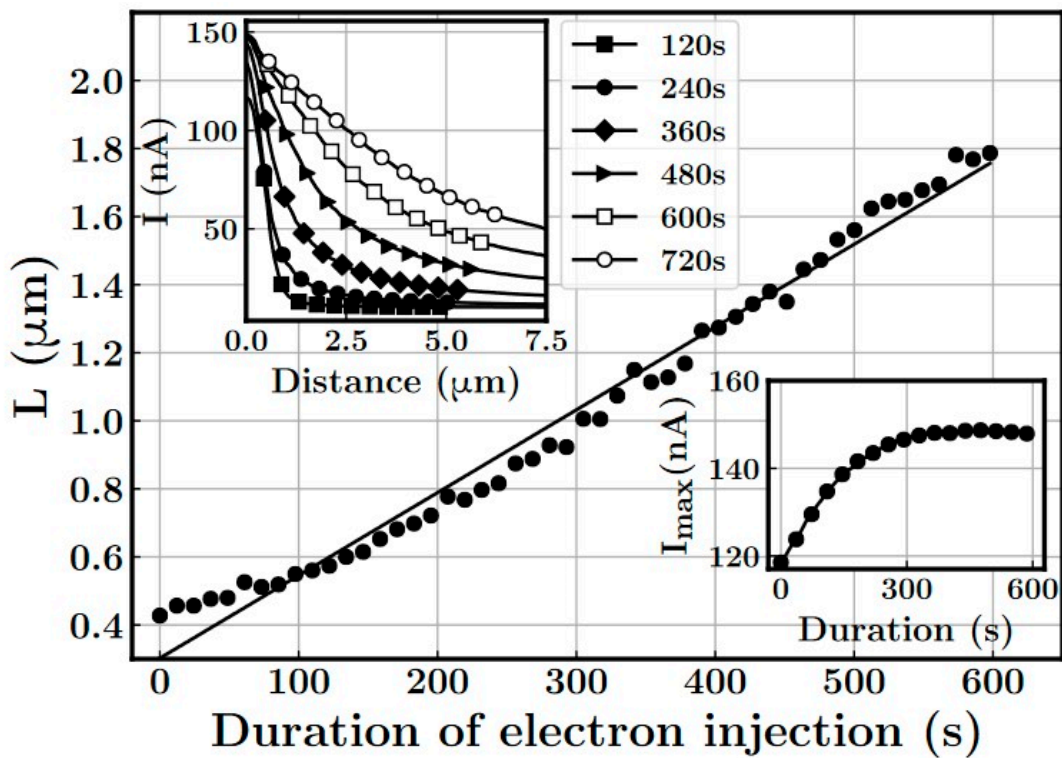


Figure 17. *L* increase as a function of electron beam injection. Inset (top): EBIC line scans for different incremental electron injection durations. Inset (bottom): electron-beam-induced current amplitude dependence on the duration of injection. Reprinted with permission from the AIP. After Ref. [26].

Figure 17 (top inset) shows the EBIC line scans for different incremental injection durations up to 720 s. Longer tails for a decay in the EBIC signal correspond to an elongated L . Simultaneously, a pronounced increase in the EBIC amplitude is observed (cf. top and bottom insets of Figure 17) and is explained by the enhanced collection efficiency of minority carriers [74–76]. I_{\max} , in the bottom inset of Figure 17, increases up to a certain value of L . Afterwards, any increase in L (cf. Figure 17, top inset) does not affect the amplitude of the induced currents. Following I_{\max} (see bottom inset of Figure 17), L saturates as well (not shown in Figure 17) and persists for more than one day at RT after the injection is stopped.

3.5. The Root Cause for the Phenomenon of Electron Injection in Gallium Oxide

Ref. [45] outlines the mechanism (cf. Figure 18) of the electron injection phenomenon for undoped GaN, which is also applicable to Ga_2O_3 :

- Direct band-to-band recombination (cf. Figure 18a,b) is not available in Ga_2O_3 due to the assumed presence of self-trapped holes. As a result, non-equilibrium electrons, which are generated by an SEM beam, are trapped by V_{Ga} and act as deep acceptors in gallium oxide (cf. Figure 18c). A fairly large concentration (10^{18} cm^{-3}) of V_{Ga} remains in the neutral state in the material, thus acting as a meta-stable electron trap. Capturing non-equilibrium electrons on V_{Ga} prevents the recombination of the non-equilibrium conduction band electrons through the trap levels (cf. Figure 18d). This results in an increased lifetime and, consequently, in a larger L [$L = (D\tau)^{1/2}$, where D is the carrier diffusivity].
- The V_{Ga} levels, which contain trapped electrons, become available again for recombination as these levels capture holes; this results in the temperature-dependent transition of trapped electrons to the valence band (cf. Figure 18e). The existence of activation energy, which prevents the near-simultaneous capture of holes by the negatively charged V_{Ga} , is noted. $\Delta E_{A,I}$ is experimentally estimated to be 91 meV.
- With an increase in hole capture on gallium vacancies, the non-equilibrium electrons in the conduction band have more chances for recombination on their respective energetic levels. This leads to a reduced τ and a slower rate of increase in L at higher temperatures, as seen in Figure 14.
- Only neutral V_{Ga} levels may trap non-equilibrium electrons. Therefore, the electrical conductivity of the sample under test is not impacted.

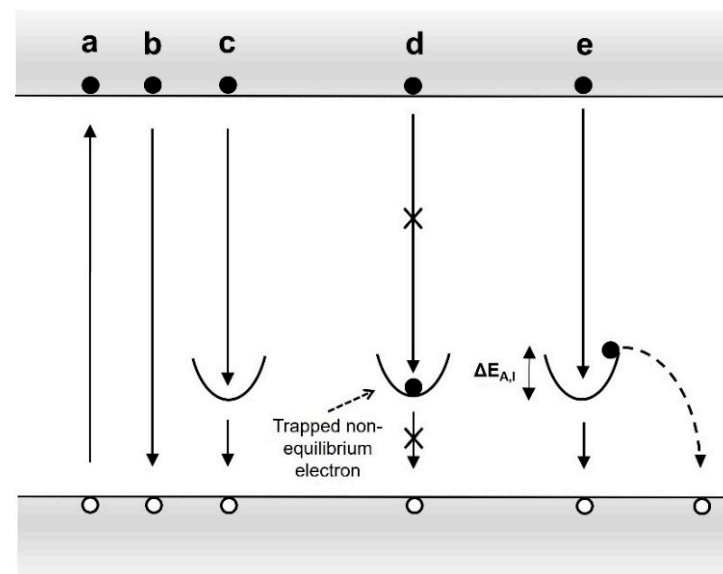


Figure 18. Model for the electron-injection-induced effect (for the example of electron beam irradiation, which generates non-equilibrium electron–hole pairs). Reprinted with permission from the American Institute of Physics. After Ref. [45].

3.6. Application of the Charge Injection Effect to Performance Control of Ga₂O₃-Based Photodetectors

Pending the fabrication of robust homoepitaxial Ga₂O₃ p–n junctions, the application of the charge injection effect to device performance enhancement is presented by the authors of this review via the example of the p-NiO/n-Ga₂O₃ heterojunction structures shown in Figure 19.

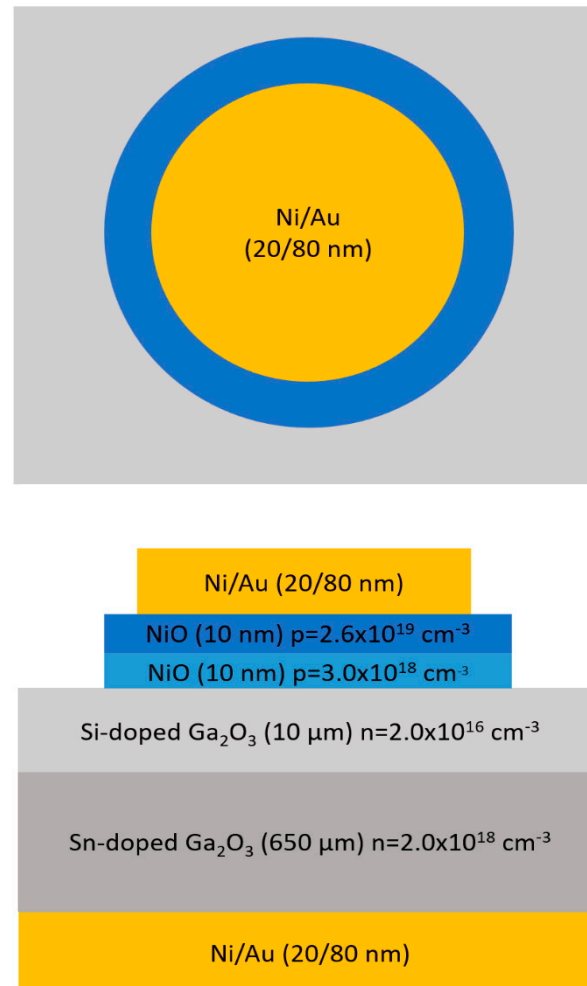


Figure 19. Architecture of the vertical p-NiO/n-Ga₂O₃ heterojunction structure (top and front view). The top Ni/Au contact is 1000 μm in diameter. The structure was provided by the group of Profs. S. J. Pearton and Fan Ren of the University of Florida.

The structures were provided by the University of Florida. They consisted of a lightly doped 10 μm layer on a conducting substrate. This layer was grown via halide vapor phase epitaxy (HVPE) on a (001) Sn-doped (10¹⁹ cm⁻³) β-Ga₂O₃ single crystal substrate. The NiO bilayer was deposited by rf (13.56 MHz) magnetron sputtering at a working pressure of 3 mTorr. The NiO bilayer consisted of a 20 nm layer, with a hole concentration $p = 10^{18} \text{ cm}^{-3}$, and a 10 nm layer, with a hole concentration $p = 2.6 \times 10^{19} \text{ cm}^{-3}$. The hole concentration in the NiO bilayer was adjusted using the Ar/O₂ ratio. The structure was then annealed at 300 °C under O₂. Finally, a top contact of 20/80 nm Ni/Au (1000 μm diameter) was deposited onto the NiO bilayer. Ohmic contacts were made to the rear surface using a Ti/Au metal stack that was deposited by e-beam evaporation followed by annealing at 550 °C for 180 s under N₂. The front surface was subjected to UV/Ozone exposure for 15 min to remove contamination prior to the metal deposition. More details regarding the fabrication and characterization of the structure can be found elsewhere [77]. It should be noted that the structure shown in Figure 19 is not optimized as a photodetector device. Therefore, the photoresponse measurements reported in this article present the

initial proof of concept for the application of the charge injection effect to bipolar Ga₂O₃-based heterojunction devices. To the best of the authors' knowledge, the results presented here are the only example currently available. Detailed studies of the application of charge injection devices are planned once bipolar gallium oxide-based homojunctions become readily available.

For the structure presented in Figure 19, the charge is injected from the p-NiO layer into that of n-Ga₂O₃, due to forward bias application (a positive bias was applied to the top nickel oxide layer for the duration of up to 600 s), thus inducing a current of 100 μ A through the structure; this corresponds to a charge density of ~ 8 nC/ μ m³ (it is two orders of magnitude larger than that, and is created by an electron beam for an increase in the diffusion length in Figures 14 and 17). The forward branch of the I–V curve for the NiO/Ga₂O₃ p–n heterojunction is shown in Figure 20, in linear and logarithmic scales. The forward turn-on voltage for the junction is ~ 1.9 V (cf. Figure 20), and is determined by the band alignment between the two materials, as reported previously in Ref. [78]. Under forward bias, the depletion layer of the p–n junction is collapsed, and holes diffuse into the Ga₂O₃. It should be noted that, because the majority electron concentration in 10 μ m-thick Ga₂O₃ is two orders of magnitude lower compared to that of the majority holes in the adjacent 10 nm-thick NiO layer, the space charge region of the NiO/Ga₂O₃ p–n junction is mostly located in n-Ga₂O₃, with a lateral extension of ~ 180 nm under zero bias. It should be additionally emphasized that, because of the structure architecture shown in Figure 19, the light-induced non-equilibrium minority carriers (holes) that contribute to the photoresponse of the heterojunction are predominantly generated in the area of n-Ga₂O₃ that is directly exposed to illumination (the stack of Ni/Au/NiO, deposited over the Ga₂O₃ layer, prevents the penetration of light down to the p–n heterojunction interface [79]). Consequently, the photoinduced holes laterally diffuse in n-Ga₂O₃ towards the space charge region of the p–n heterojunction, where they are swept and collected by the built-in electric field (estimated at 0.8 MV.cm^{−1}) and thus contribute to a photosignal. In contrast to minority holes, because of the direction of the built-in electric field, non-equilibrium photo-induced majority electrons are not collected and eventually recombine. Therefore, a p–n heterojunction is a minority carrier device.

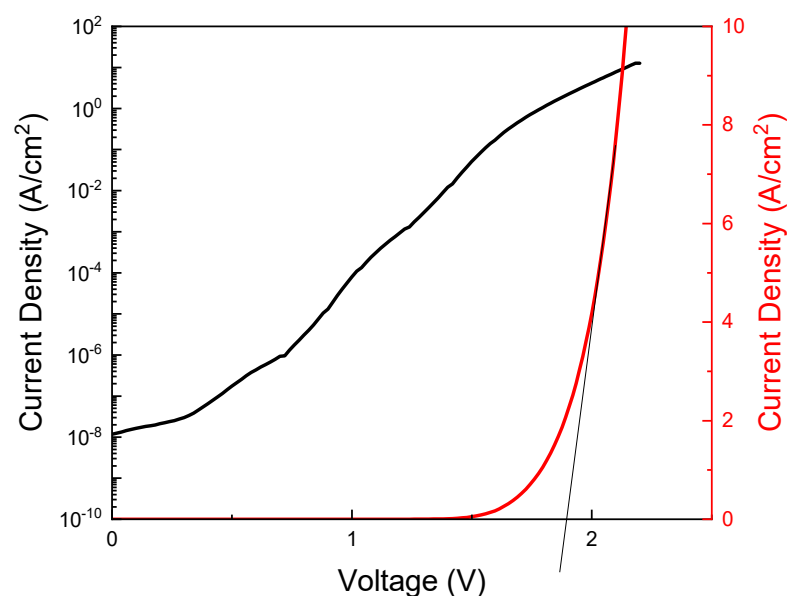


Figure 20. Forward branch of the I–V curve for the p-NiO/n-Ga₂O₃ heterojunction in linear and logarithmic scales. The turn-on voltage value, obtained by the intersection of the tangential line to the I–V curve with the horizontal axis, is ~ 1.9 V.

Similar to the electron beam injection in Figures 14 and 17, the forward bias charge injection results in an increase in the minority carrier diffusion length in the 10 μ m-thick

gallium oxide layer. Although L was not directly measured, the more than 200% increase in the peak photoresponse that is shown in Figure 21 provides experimental evidence for its elongation. Ref. [32] reported a similar photoresponse enhancement in the forward-biased GaN p–n junction and suggested the mechanism implicated in this effect. The application of forward bias to the NiO/Ga₂O₃ p–n junction results in a decrease in the potential barrier (~ 1.03 V for built-in voltage, V_{bi}) at the interface of two semiconducting layers. As a result, the holes from p-NiO are injected into n-Ga₂O₃ and likely become captured by meta-stable traps. Although the exact energetic location for these possible traps is yet unknown, Ref. [80] reports a trapping level for holes in n-type Ga₂O₃; this is located 140 meV above the top of the valence band. This level was revealed by the deep level transient spectroscopy (DLTS) technique during a study of hole injection via trap-assisted tunneling from p⁺-NiO into n-Ga₂O₃ under forward bias. Capturing injected charge carriers on the meta-stable energetic levels prevents the recombination of light-induced non-equilibrium carriers in n-type gallium oxide through these levels. As a result, the non-equilibrium carriers remain in the respective valence and conduction bands of Ga₂O₃ for a longer time, thus leading to a larger τ and, therefore, a longer diffusion length, L ; thus in agreement with the model in Figure 18. A longer L dictates an enhanced collection efficiency and photoresponse.

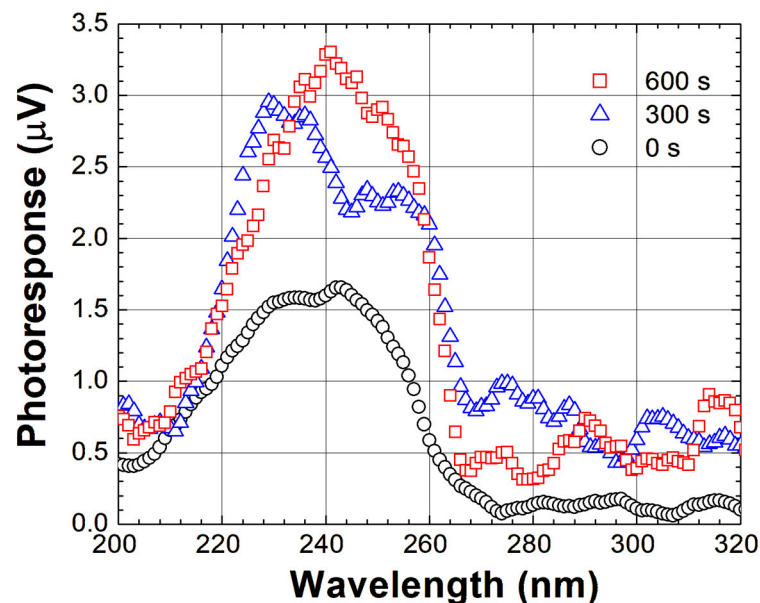


Figure 21. Spectral photoresponse of the structure in Figure 19 before and after incremental charge injection. The charge, corresponding to 600 s of injection, is 60 mC. The effect persists for at least several hours.

It should be noted that while it takes only 600 s to induce the enhancement of the photoresponse presented in Figure 21, the relaxation of its peak value to the pre-injection level occurs within roughly 6000 s. This, on the one hand, indicates that the device performance can be controlled by solid-state charge injection and, on the other hand, provides additional evidence for the metastability of traps involved in the phenomenon of interest. Detailed studies on the application of charge injection-induced effects in gallium oxide-based photodetectors are under way.

4. Summary

In summary, while irradiation with energetic particles and an increase in temperature lead to a decrease in the minority carrier diffusion length, charge injection using SEM beam mitigates the negative influence of radiation on carrier recombination in Ga₂O₃. It is demonstrated that L , reduced as a result of energetic particle bombardment, could

be returned to its initial value, or even increased above it. This effect was attributed to non-equilibrium carrier trapping on native defects and the consequent increase in τ .

Careful sample inspection using high magnification scanning electron microscopy did not reveal any changes in the surface morphology of Ga₂O₃ irradiated with 1.5 MeV electrons, 10 MeV protons, or 18 MeV alpha-particles compared to the reference sample. It should be additionally emphasized that SEM electron beam injection, which is employed to induce an increase in the diffusion length, does not lead to the polarization of the samples due to a buildup of charge, as the samples are grounded. The trapping of charges, which affects the minority carrier lifetime and diffusion length, is related to electron-beam-induced non-equilibrium carriers, but not to primary (SEM beam) electrons. Therefore, the sample's electroneutrality is always preserved. Finally, while L and τ are affected by charge injection, the minority carrier mobility remains unchanged. A detailed discussion of the impact of low-energy electron beam irradiation on carrier mobility is given in Ref. [22].

With Ga₂O₃ p–n homojunctions becoming feasible, a solid-state charge injection caused by bias will be employed (as in Figures 19–21), thus paving the road towards the purely electrical (athermal) mitigation of radiation-induced defects in bipolar devices. Detailed studies of device performance (photoresponse) under variable temperatures and forward current magnitudes and durations will allow optimum regimes for the application of the effect of interest to be obtained. This will be the subject of future work.

Author Contributions: Conceptualization, L.C.; methodology, S.M. and A.S.; software, A.S.; validation, A.S. and S.M.; formal analysis, S.M.; investigation, S.M.; writing—original draft preparation, L.C.; writing—review and editing, L.C. and A.R.; supervision, L.C.; project administration, L.C.; funding acquisition, L.C. All authors have read and agreed to the published version of the manuscript.

Funding: This research was supported in part by the US-Israel Binational Science Foundation (Awards No. 2022056 and 2022779), the National Science Foundation (ECCS #2310285), and NATO (G5748).

Data Availability Statement: The data presented in this review are openly available from the articles cited in this review paper, as well as from the corresponding author upon request.

Conflicts of Interest: The authors declare no conflicts of interest.

References

1. Pearton, S.J.; Yang, J.; Cary, P.H.; Ren, F.; Kim, J.; Tadjer, M.J.; Mastro, M.A. A review of Ga₂O₃ materials, processing, and devices. *Appl. Phys. Rev.* **2018**, *5*, 011301. [[CrossRef](#)]
2. Baliga, B.J. Gallium nitride devices for power electronic applications. *Semicond. Sci. Technol.* **2013**, *28*, 074011. [[CrossRef](#)]
3. Chernyak, L.; Osinsky, A.; Schulte, A. Minority carrier transport in GaN and related materials. *Solid-State Electron.* **2001**, *45*, 1687–1702. [[CrossRef](#)]
4. Polyakov, A.Y.; Smirnov, N.B.; Shchemerov, I.V.; Pearton, S.J.; Ren, F.; Chernykh, A.V.; Kochkova, A.I. Electrical properties of bulk semi-insulating β -Ga₂O₃ (Fe). *Appl. Phys. Lett.* **2018**, *113*, 142102. [[CrossRef](#)]
5. Gao, H.; Muralidharan, S.; Pronin, N.; Karim, M.R.; White, S.M.; Asel, T.; Foster, G.; Krishnamoorthy, S.; Rajan, S.; Cao, L.R.; et al. Optical signatures of deep level defects in Ga₂O₃. *Appl. Phys. Lett.* **2018**, *112*, 242102. [[CrossRef](#)]
6. Yang, J.; Ren, F.; Pearton, S.J.; Yang, G.; Kim, J.; Kuramata, A. 1.5 MeV electron irradiation damage in β -Ga₂O₃ vertical rectifiers. *J. Vac. Sci. Technol. B Nanotechnol. Microelectron.* **2017**, *35*, 4. [[CrossRef](#)]
7. Mock, A.; Korlacki, R.; Briley, C.; Darakchieva, V.; Monemar, B.; Kumagai, Y.; Goto, K.; Higashiwaki, M.; Schubert, M. Band-to-band transitions, selection rules, effective mass, and excitonic contributions in monoclinic β -Ga₂O₃. *Phys. Rev. B* **2017**, *96*, 14. [[CrossRef](#)]
8. Mastro, M.A.; Kuramata, A.; Calkins, J.; Kim, J.; Ren, F.; Pearton, S.J. Perspective—Opportunities and Future Directions for Ga₂O₃. *ECS J. Solid State Sci. Technol.* **2017**, *6*, P356–P359. [[CrossRef](#)]
9. Stepanov, S.I.; Nikolaev, V.I.; Bougrov, V.E.; Romanov, A.E. Gallium Oxide: Properties and Applications—A Review. *Rev. Adv. Mater. Sci.* **2016**, *44*, 63–86.
10. Chikoidze, E.; Sartet, C.; Mohamed, H.; Madaci, I.; Tchelidze, T.; Modreanu, M.; Vales-Castro, P.; Rubio, C.; Arnold, C.; Sallet, V.; et al. Enhancing the intrinsic p-type conductivity of the ultra-wide bandgap Ga₂O₃ semiconductor. *J. Mater. Chem. C* **2019**, *7*, 10231–10239. [[CrossRef](#)]
11. Chi, Z.; Sartet, C.; Zheng, Y.; Modak, S.; Chernyak, L.; Schaefer, C.M.; Padilla, J.; Santiso, J.; Ruzin, A.; Gonçalves, A.M.; et al. Native defects association enabled room-temperature p-type conductivity in β -Ga₂O₃. *J. Alloys Compd.* **2023**, *969*, 172454. [[CrossRef](#)]

12. Kananen, B.E.; Giles, N.C.; Halliburton, L.E.; Foundos, G.K.; Chang, K.B.; Stevens, K.T. Self-trapped holes in β -Ga₂O₃ crystals. *J. Appl. Phys.* **2017**, *122*, 6. [[CrossRef](#)]
13. Varley, J.B.; Janotti, A.; Franchini, C.; Van de Walle, C.G. Role of self-trapping in luminescence and p-type conductivity of wide-band-gap oxides. *Phys. Rev. B* **2012**, *85*, 081109. [[CrossRef](#)]
14. Yoshioka, S.; Hayashi, H.; Kuwabara, A.; Oba, F.; Matsunaga, K.; Tanaka, I. Structures and energetics of Ga₂O₃ polymorphs. *J. Phys. Condens. Matter* **2007**, *19*, 11. [[CrossRef](#)]
15. He, H.; Orlando, R.; Blanco, M.A.; Pandey, R.; Amzallag, E.; Baraille, I.; Rérat, M. First-principles study of the structural, electronic, and optical properties of Ga₂O₃ in its monoclinic and hexagonal phases. *Phys. Rev. B* **2006**, *74*, 8. [[CrossRef](#)]
16. He, H.; Blanco, M.A.; Pandey, R. Electronic and thermodynamic properties of β -Ga₂O₃. *Appl. Phys. Lett.* **2006**, *88*, 261904. [[CrossRef](#)]
17. Furthmüller, J.; Bechstedt, F. Quasiparticle bands and spectra of Ga₂O₃ polymorphs. *Phys. Rev. B* **2016**, *93*, 115204. [[CrossRef](#)]
18. Chernyak, L.; Schulte, A. Method and System for Performance Improvement of Photodetectors and Solar. Cells. Patent U.S. Patent 6,674,064, 6 January 2004.
19. Lopatiuk-Tirpak, O.; Chernyak, L.; Xiu, F.X.; Liu, J.L.; Jang, S.; Ren, F.; Pearton, S.J.; Gartsman, K.; Feldman, Y.; Osinsky, A.; et al. Studies of minority carrier diffusion length increase in p-type ZnO:Sb. *J. Appl. Phys.* **2006**, *100*, 086101. [[CrossRef](#)]
20. Chernyak, L.; Osinsky, A.; Nootz, G.; Schulte, A.; Jasinski, J.; Benamara, M.; Liliental-Weber, Z.; Look, D.C.; Molnar, R.J. Electron beam and optical depth profiling of quasibulk GaN. *Appl. Phys. Lett.* **2000**, *77*, 2695–2697. [[CrossRef](#)]
21. Chernyak, L.; Nootz, G.; Osinsky, A. Enhancement of minority carrier transport in forward biased GaN p-n junction. *Electron. Lett.* **2001**, *37*, 922–923. [[CrossRef](#)]
22. Chernyak, L.; Osinsky, A.; Fuflyigin, V.; Schubert, E.F. Electron beam-induced increase of electron diffusion length in p-type GaN and AlGaIn/GaN superlattices. *Appl. Phys. Lett.* **2000**, *77*, 875–877. [[CrossRef](#)]
23. Lopatiuk-Tirpak, O.; Chernyak, L.; Wang, Y.L.; Ren, F.; Pearton, S.J.; Gartsman, K.; Feldman, Y. Cathodoluminescence studies of carrier concentration dependence for the electron irradiation effects in p-GaN. *Appl. Phys. Lett.* **2007**, *90*, 3. [[CrossRef](#)]
24. Lopatiuk-Tirpak, O.; Chernyak, L.; Mandalapu, L.J.; Yang, Z.; Liu, J.L.; Gartsman, K.; Feldman, Y.; Dashevsky, Z. Influence of electron injection on the photoresponse of ZnO homojunction diodes. *Appl. Phys. Lett.* **2006**, *89*, 142114. [[CrossRef](#)]
25. Modak, S.; Chernyak, L.; Khodorov, S.; Lubomirsky, I.; Yang, J.; Ren, F.; Pearton, S.J. Impact of Electron Injection and Temperature on Minority Carrier Transport in Alpha-Irradiated β -Ga₂O₃ Schottky Rectifiers. *ECS J. Solid State Sci. Technol.* **2019**, *8*, Q3050. [[CrossRef](#)]
26. Modak, S.; Lee, J.; Chernyak, L.; Yang, J.; Ren, F.; Pearton, S.J.; Khodorov, S.; Lubomirsky, I. Electron injection-induced effects in Si-doped β -Ga₂O₃. *AIP Adv.* **2019**, *9*, 015127. [[CrossRef](#)]
27. Modak, S.; Schulte, A.; Sartel, C.; Sallet, V.; Dumont, Y.; Chikoidze, E.; Xia, X.; Ren, F.; Pearton, S.J.; Ruzin, A.; et al. Impact of radiation and electron trapping on minority carrier transport in p-Ga₂O₃. *Appl. Phys. Lett.* **2022**, *120*, 233503. [[CrossRef](#)]
28. Chernyak, L.; Burdett, W.; Klimov, M.; Osinsky, A. Cathodoluminescence studies of the electron injection-induced effects in GaN. *Appl. Phys. Lett.* **2003**, *82*, 3680–3682. [[CrossRef](#)]
29. Lopatiuk, O.; Burdett, W.; Chernyak, L.; Ip, K.P.; Heo, Y.W.; Norton, D.P.; Pearton, S.J.; Hertog, B.; Chow, P.P.; Osinsky, A. Minority carrier transport in p-type Zn_{0.9}Mg_{0.1}O doped with phosphorus. *Appl. Phys. Lett.* **2005**, *86*, 012105. [[CrossRef](#)]
30. Lopatiuk, O.; Chernyak, L.; Osinsky, A.; Xie, J.Q. Lithium-related states as deep electron traps in ZnO. *Appl. Phys. Lett.* **2005**, *87*, 214110. [[CrossRef](#)]
31. Lopatiuk-Tirpak, O.; Nootz, G.; Flitsiyan, E.; Chernyak, L.; Mandalapu, L.J.; Yang, Z.; Liu, J.L.; Gartsman, K.; Osinsky, A. Influence of electron injection on the temporal response of ZnO homojunction photodiodes. *Appl. Phys. Lett.* **2007**, *91*, 042115. [[CrossRef](#)]
32. Chernyak, L.; Schulte, A.; Osinsky, A.; Graff, J.; Schubert, E.F. Influence of electron injection on performance of GaN photodetectors. *Appl. Phys. Lett.* **2002**, *80*, 926–928. [[CrossRef](#)]
33. Lee, J.; Flitsiyan, E.; Chernyak, L.; Yang, J.; Ren, F.; Pearton, S.J.; Meyler, B.; Salzman, Y.J. Effect of 1.5 MeV electron irradiation on β -Ga₂O₃ carrier lifetime and diffusion length. *Appl. Phys. Lett.* **2018**, *112*, 5. [[CrossRef](#)]
34. Modak, S.; Chernyak, L.; Schulte, A.; Xian, M.; Ren, F.; Pearton, S.J.; Lubomirsky, I.; Ruzin, A.; Kosolobov, S.S.; Drachev, V.P. Electron beam probing of non-equilibrium carrier dynamics in 18 MeV alpha particle- and 10 MeV proton-irradiated Si-doped β -Ga₂O₃ Schottky rectifiers. *Appl. Phys. Lett.* **2021**, *118*, 202105. [[CrossRef](#)]
35. Modak, S.; Chernyak, L.; Khodorov, S.; Lubomirsky, I.; Ruzin, A.; Xian, M.; Ren, F.; Pearton, S.J. Effect of Electron Injection on Minority Carrier Transport in 10 MeV Proton Irradiated β -Ga₂O₃ Schottky Rectifiers. *ECS J. Solid State Sci. Technol.* **2020**, *9*, 045018. [[CrossRef](#)]
36. Modak, S.; Chernyak, L.; Schulte, A.; Sartel, C.; Sallet, V.; Dumont, Y.; Chikoidze, E.; Xia, X.; Ren, F.; Pearton, S.J.; et al. Variable temperature probing of minority carrier transport and optical properties in p-Ga₂O₃. *APL Mater.* **2022**, *10*, 031106. [[CrossRef](#)]
37. Dimitriadis, C.A. Determination of bulk diffusion length in thin semiconductor layers by SEM-EBIC. *J. Phys. D Appl. Phys.* **1981**, *14*, 2269–2274. [[CrossRef](#)]
38. Chernyak, L.; Osinsky, A.; Temkin, H.; Yang, J.W.; Chen, Q.; Asif Khan, M. Electron beam induced current measurements of minority carrier diffusion length in gallium nitride. *Appl. Phys. Lett.* **1996**, *69*, 2531–2533. [[CrossRef](#)]
39. Yakimov, E.B.; Polyakov, A.Y.; Smirnov, N.B.; Shchemerov, I.V.; Yang, J.; Ren, F.; Yang, G.; Kim, J.; Pearton, S.J. Diffusion length of non-equilibrium minority charge carriers in β -Ga₂O₃ measured by electron beam induced current. *J. Appl. Phys.* **2018**, *123*, 185704. [[CrossRef](#)]

40. Ma, N.; Tanen, N.; Verma, A.; Guo, Z.; Luo, T.; Xing, H.; Jena, D. Intrinsic electron mobility limits in β -Ga₂O₃. *Appl. Phys. Lett.* **2016**, *109*, 212101. [[CrossRef](#)]
41. Polyakov, A.Y.; Lee, I.-H.; Smirnov, N.B.; Yakimov, E.B.; Shchemerov, I.V.; Chernykh, A.V.; Kochkova, A.I.; Vasilev, A.A.; Ren, F.; Carey, P.H.; et al. Hydrogen plasma treatment of β -Ga₂O₃: Changes in electrical properties and deep trap spectra. *Appl. Phys. Lett.* **2019**, *115*, 032101. [[CrossRef](#)]
42. Polyakov, A.Y.; Smirnov, N.B.; Shchemerov, I.V.; Yakimov, E.B.; Pearton, S.J.; Fares, C.; Yang, J.; Ren, F.; Kim, J.; Lagov, P.B.; et al. Defects responsible for charge carrier removal and correlation with deep level introduction in irradiated β -Ga₂O₃. *Appl. Phys. Lett.* **2018**, *113*, 092102. [[CrossRef](#)]
43. Adnan, M.M.R.; Verma, D.; Xia, Z.; Kalarickal, N.K.; Rajan, S.; Myers, R.C. Spectral Measurement of the Breakdown Limit of β -Ga₂O₃ and Tunnel Ionization of Self-Trapped Excitons and Holes. *Phys. Rev. Appl.* **2021**, *16*, 034011. [[CrossRef](#)]
44. Chi, Z.; Sartel, C.; Zheng, Y.; Modak, S.; Chernyak, L.; Schaefer, C.M.; Padilla, J.; Santiso, J.; Ruzin, A.; Goncalves, A.M.; et al. Native defect association in beta-Ga₂O₃ enables room-temperature p-type conductivity. *arXiv* **2023**, arXiv:2306.01115.
45. Modak, S.; Chernyak, L.; Xian, M.; Ren, F.; Pearton, S.J.; Khodorov, S.; Lubomirsky, I.; Ruzin, A.; Dashevsky, Z. Impact of electron injection on carrier transport and recombination in unintentionally doped GaN. *J. Appl. Phys.* **2020**, *128*, 085702. [[CrossRef](#)]
46. Leamy, H.J. Charge collection scanning electron microscopy. *J. Appl. Phys.* **1982**, *53*, R51–R80. [[CrossRef](#)]
47. Ahn, S.; Lin, Y.-H.; Ren, F.; Oh, S.; Jung, Y.; Yang, G.; Kim, J.; Mastro, M.A.; Hite, J.K.; Eddy, C.R.; et al. Effect of 5 MeV proton irradiation damage on performance of β -Ga₂O₃ photodetectors. *J. Vac. Sci. Technol. B Nanotechnol. Microelectron.* **2016**, *34*, 5. [[CrossRef](#)]
48. Armstrong, A.M.; Crawford, M.H.; Jayawardena, A.; Ahyi, A.; Dhar, S. Role of self-trapped holes in the photoconductive gain of β -gallium oxide Schottky diodes. *J. Appl. Phys.* **2016**, *119*, 103102. [[CrossRef](#)]
49. Yamaoka, S.; Nakayama, M. Evidence for formation of self-trapped excitons in a β -Ga₂O₃ single crystal. *Phys. Status Solidi (C)* **2016**, *13*, 93–96. [[CrossRef](#)]
50. Yamaoka, S.; Furukawa, Y.; Nakayama, M. Initial process of photoluminescence dynamics of self-trapped excitons in a β -Ga₂O₃ single crystal. *Phys. Rev. B* **2017**, *95*, 094304. [[CrossRef](#)]
51. Yamaoka, S.; Mikuni, Y.; Nakayama, M. Photoluminescence polarization characteristics of self-trapped excitons in an undoped β -Ga₂O₃ single crystal. *J. Phys. Conf. Ser.* **2019**, *1220*, 012030. [[CrossRef](#)]
52. Frodason, Y.K.; Johansen, K.M.; Vines, L.; Varley, J.B. Self-trapped hole and impurity-related broad luminescence in β -Ga₂O₃. *J. Appl. Phys.* **2020**, *127*, 075701. [[CrossRef](#)]
53. Marcinkevičius, S.; Speck, J.S. Ultrafast dynamics of hole self-localization in β -Ga₂O₃. *Appl. Phys. Lett.* **2020**, *116*, 132101. [[CrossRef](#)]
54. Binet, L.; Gourier, D. Origin of the blue luminescence of β -Ga₂O₃. *J. Phys. Chem. Solid* **1998**, *59*, 1241–1248. [[CrossRef](#)]
55. Blasse, G.; Brill, A. Some observations on the luminescence of β -Ga₂O₃. *J. Phys. Chem. Solids* **1970**, *31*, 707–711. [[CrossRef](#)]
56. Oishi, T.; Koga, Y.; Harada, K.; Kasu, M. High-mobility β -Ga₂O₃ single crystals grown by edge-defined film-fed growth method and their Schottky barrier diodes with Ni contact. *Appl. Phys. Express* **2015**, *8*, 3. [[CrossRef](#)]
57. Irmscher, K.; Galazka, Z.; Pietsch, M.; Uecker, R.; Fornari, R. Electrical properties of β -Ga₂O₃ single crystals grown by the Czochralski method. *J. Appl. Phys.* **2011**, *110*, 7. [[CrossRef](#)]
58. Lee, J.; Flitsyan, E.; Chernyak, L.; Ahn, S.; Ren, F.; Yuna, L.; Pearton, S.J.; Kim, J.; Meyler, B.; Salzman, J. Optical Signature of the Electron Injection in Ga₂O₃. *ECS J. Solid State Sci. Technol.* **2016**, *6*, Q3049. [[CrossRef](#)]
59. Modak, S.; Chernyak, L.; Schulte, A.; Xian, M.; Ren, F.; Pearton, S.J.; Ruzin, A.; Kosolobov, S.S.; Drachev, V.P. Temperature dependence of cathodoluminescence emission in irradiated Si-doped β -Ga₂O₃. *AIP Adv.* **2021**, *11*, 125014. [[CrossRef](#)]
60. Yu, P.; Cardona, M. *Fundamentals of Semiconductors; Graduate Texts in Physics*; Springer: Berlin/Heidelberg, Germany, 2010.
61. Yang, J.; Ren, F.; Khanna, R.; Bevin, K.; Geerpuram, D.; Tung, L.-C.; Lin, J.; Jiang, H.; Lee, J.; Flitsyan, E.; et al. Annealing of dry etch damage in metallized and bare (-201) Ga₂O₃. *J. Vac. Sci. Technol. B Nanotechnol. Microelectron.* **2017**, *35*, 5. [[CrossRef](#)]
62. Yang, J.; Fares, C.; Guan, Y.; Ren, F.; Pearton, S.J.; Bae, J.; Kim, J.; Kuramata, A. Eighteen mega-electron-volt alpha-particle damage in homoepitaxial β -Ga₂O₃ Schottky rectifiers. *J. Vac. Sci. Technol. B* **2018**, *36*, 031205. [[CrossRef](#)]
63. Yang, J.; Chen, Z.; Ren, F.; Pearton, S.J.; Yang, G.; Kim, J.; Lee, J.; Flitsyan, E.; Chernyak, L.; Kuramata, A. 10 MeV proton damage in β -Ga₂O₃ Schottky rectifiers. *J. Vac. Sci. Technol. B Nanotechnol. Microelectron.* **2018**, *36*, 011206. [[CrossRef](#)]
64. Eckstein, M.; Habermeier, H.U. Numerical Analysis of the Temperature Dependence of Ebc and Cl Contrasts. *Le J. de Phys. IV* **1991**, *1*, C6. [[CrossRef](#)]
65. Modak, S.; Chernyak, L.; Lubomirsky, I.; Khodorov, S. Continuous and Time-Resolved Cathodoluminescence Studies of Electron Injection Induced Effects in Gallium Nitride. In Proceedings of the Advanced Technologies for Security Applications, Leuven, Belgium, 17–18 September 2019; Springer: Dordrecht, The Netherlands; pp. 109–117.
66. Lin, Y.; Flitsyan, E.; Chernyak, L.; Malinauskas, T.; Aleksiejunas, R.; Jarasiunas, K.; Lim, W.; Pearton, S.J.; Gartsman, K. Optical and electron beam studies of carrier transport in quasibulk GaN. *Appl. Phys. Lett.* **2009**, *95*, 092101. [[CrossRef](#)]
67. Godlewski, M.; Lusakowska, E.; Goldys, E.M.; Phillips, M.R.; Bottcher, T.; Figge, S.; Hommel, D.; Prystawko, P.; Leszcynski, M.; Grzegory, I.; et al. Diffusion length of carriers and excitons in GaN-influence of epilayer microstructure. *Appl. Surf. Sci.* **2004**, *223*, 294–302. [[CrossRef](#)]
68. Cojocar, L.N. Defect-annealing in neutron-damaged β -Ga₂O₃. *Radiat. Eff.* **2006**, *21*, 157–160. [[CrossRef](#)]

69. Polyakov, A.Y.; Smirnov, N.B.; Shchemerov, I.V.; Yakimov, E.B.; Yang, J.; Ren, F.; Yang, G.; Kim, J.; Kuramata, A.; Pearton, S.J. Point defect induced degradation of electrical properties of Ga₂O₃ by 10 MeV proton damage. *Appl. Phys. Lett.* **2018**, *112*, 032107. [[CrossRef](#)]
70. Kim, J.; Pearton, S.J.; Fares, C.; Yang, J.; Ren, F.; Kim, S.; Polyakov, A.Y. Radiation damage effects in Ga₂O₃ materials and devices. *J. Mater. Chem. C* **2019**, *7*, 10–24. [[CrossRef](#)]
71. Pearton, S.J.; Aitkaliyeva, A.; Xian, M.; Ren, F.; Khachatryan, A.; Ildefonso, A.; Islam, Z.; Jafar Rasel, M.A.; Haque, A.; Polyakov, A.Y.; et al. Review—Radiation Damage in Wide and Ultra-Wide Bandgap Semiconductors. *ECS J. Solid State Sci. Technol.* **2021**, *10*, 055008. [[CrossRef](#)]
72. Yakimov, E.B.; Polyakov, A.Y.; Shchemerov, I.V.; Smirnov, N.B.; Vasilev, A.A.; Vergeles, P.S.; Yakimov, E.E.; Chernykh, A.V.; Ren, F.; Pearton, S.J. Experimental estimation of electron–hole pair creation energy in β-Ga₂O₃. *Appl. Phys. Lett.* **2021**, *118*, 202106. [[CrossRef](#)]
73. Karjalainen, A.; Weiser, P.M.; Makkonen, I.; Reinertsen, V.M.; Vines, L.; Tuomisto, F. Interplay of vacancies, hydrogen, and electrical compensation in irradiated and annealed n-type β-Ga₂O₃. *J. Appl. Phys.* **2021**, *129*, 165702. [[CrossRef](#)]
74. Ledra, M.; Tabet, N. Monte Carlo simulation of the EBIC collection efficiency of a Schottky nanocontact. *Superlattices Microstruct.* **2009**, *45*, 444–450. [[CrossRef](#)]
75. Yakimov, E.B.; Borisov, S.S.; Zaitsev, S.I. EBIC measurements of small diffusion length in semiconductor structures. *Semiconductors* **2007**, *41*, 411–413. [[CrossRef](#)]
76. Donolato, C. Modeling the Ebic Measurements of Diffusion Lengths and the Recombination Contrast at Extended Defects. *J. phys., Colloq.* **1989**, *50*, C6-57–C6-64. [[CrossRef](#)]
77. Li, J.-S.; Xia, X.; Chiang, C.-C.; Hays, D.C.; Gila, B.P.; Craciun, V.; Ren, F.; Pearton, S.J. Deposition of sputtered NiO as a p-type layer for heterojunction diodes with Ga₂O₃. *J. Vac. Sci. Technol. A* **2023**, *41*, 013405. [[CrossRef](#)]
78. Vasquez, J.M.T.; Ashai, A.; Lu, Y.; Khandelwal, V.; Rajbhar, M.; Kumar, M.; Li, X.; Sarkar, B. A self-powered and broadband UV PIN photodiode employing a NiO_x layer and a β-Ga₂O₃ heterojunction. *J. Phys. D Appl. Phys.* **2023**, *56*, 065104. [[CrossRef](#)]
79. Gong, H.; Chen, X.; Xu, Y.; Chen, Y.; Ren, F.; Liu, B.; Gu, S.; Zhang, R.; Ye, J. Band Alignment and Interface Recombination in NiO/β-Ga₂O₃ Type-II p-n Heterojunctions. *IEEE Trans. Electron. Devices* **2020**, *67*, 3341. [[CrossRef](#)]
80. Verma, D. Measurement of Local Electric Fields and the Onset of Breakdown in Ultra-Wide Band Gap Semiconductor Devices Using Photocurrent Spectroscopy. Ph.D. Dissertation, The Ohio State University, Columbus, OH, USA, 2023.

Disclaimer/Publisher’s Note: The statements, opinions and data contained in all publications are solely those of the individual author(s) and contributor(s) and not of MDPI and/or the editor(s). MDPI and/or the editor(s) disclaim responsibility for any injury to people or property resulting from any ideas, methods, instructions or products referred to in the content.